PHILOSOPHICAL TRANSACTIONS OF THE ROYAL SOCIETY A MATHEMATICAL, PHYSICAL & ENGINEERING SCIENCES

The Role of Continuum Damage in Creep Crack Growth

D. R. Hayhurst, P. R. Brown and C. J. Morrison

Phil. Trans. R. Soc. Lond. A 1984 **311**, 131-158
doi: 10.1098/rsta.1984.0022

Phil. Trans. R. Soc. Lond. A **311**, 131–158 (1984) [131]
Printed in Great Britain

THE ROLE OF CONTINUUM DAMAGE IN CREEP CRACK GROWTH

BY D. R. HAYHURST, P. R. BROWN AND C. J. MORRISON
University of Leicester, Engineering Department, Leicester LE1 7RH, U.K.

(*Communicated by B. A. Bilby, F.R.S. – Received 27 June 1983*)

[Plates 1–7]

CONTENTS

Theories that have been used to predict the rate of growth of cracks due to creep are reviewed and assessed. The need is expressed for a sounder understanding of the mechanisms by which creep crack growth takes place. The aim of this paper is to answer the question: can continuum damage mechanics provide the mechanism by which cracks grow by creep? The paper reports the results of theoretical and experimental studies on internally and externally cracked, plane strain, tension members, in an aluminium alloy, in copper and in 316 stainless steel, all of which undergo high temperature creep rupture under steady loads. Theoretical predictions of lifetimes, expressed as a representative rupture stress, of damage fields and of crack growth are made by using a previously developed finite element system (Hayhurst, Dimmer & Morrison, *Phil. Trans. R. Soc. Lond.* **311**, 103 (1984)) based on the theory of continuum damage mechanics.

The theoretical predictions are shown to be in close agreement with experimental observations. The effect of the growth of continuum damage is to produce considerable stress redistribution and to cause the nullification of stress singularities. The multi-axial stress rupture criterion of the material plays an important role in the determination of lifetimes and of the planes upon which crack propagation takes place. The numerical solution procedure is automatic but requires that the constitutive equations model the elastic response, the creep strain rates, including tertiary behaviour, and the multi-axial stress rupture criterion of the material at the appropriate stress levels.

Continuum damage mechanics theory is shown to be capable of modelling the propagation of cracks through material which has suffered relatively low damage.

1. Introduction

(*a*) *Technological background*

Fracture mechanics is used in the design of structural components, which operate below the creep range, to determine the conditions under which a defect may become unstable and propagate. For a particular geometry and set of loading conditions the size of the defect which results in unstable propagation is known as the critical length. In high strength metallic alloys, where little plastic deformation takes place in a conventional uni-axial stress–strain test before fracture, unstable crack propagation occurs while plasticity is confined to the crack tip region; the behaviour is dominated by the surrounding elastic field and the values of the critical crack length are obtained from linear elastic fracture mechanics (l.e.f.m.) by using a critical value of the stress intensity factor K_{Ic}. In the case of lower strength, or tougher materials widespread plasticity can take place before the initiation of the fracture process; the behaviour is influenced by extensive plasticity in the body and estimates of the critical crack length, at initiation, are based on post yield fracture mechanics (p.y.f.m.) with a critical value of a parameter J_{Ic} related to the J contour integral described by Rice (1968).

The development of a fracture mechanics that may be used to determine the rate of propagation of cracks due to high-temperature creep under conditions of steady load has reached a primitive stage when compared with the advanced stage of development of l.e.f.m. and p.y.f.m. Typically, cracked structures operate at low stresses (under $0.25\sigma_y$), where σ_y is the uni-axial yield stress, and they are designed for a lifetime of typically 2×10^5 h; at one extreme a crack may be small relative to the load bearing section, in which it is contained, and at the other extreme it may occupy a significant fraction of the load bearing section, so that, depending on the material of the structure, a broad range of crack velocities may be observed. At the higher temperatures, typically $0.5T_m$, where T_m is the melting temperature of the base metal, the problem reduces to one of the determination of the time required for an existing defect or crack to grow to its critical

length. Although high-temperature design codes (B.S. 5500 (1982) and American Society for Mechanical Engineers, code case N47 (1977)) make no specific recommendations for the design of defective components, techniques have been developed for the prediction of creep crack growth rates which have been checked against the results of experiments done on cracked laboratory specimens. These techniques are now discussed.

(*b*) *Phenomenological theories of crack growth*

Three approaches have been widely used. In the first, proposed by Neate & Siverns (1973), it is assumed that the crack growth rate is proportional to $(K_I)^s$, where K_I is the value of the stress intensity factor obtained from l.e.f.m. for the current crack length and s is a constant which is close in value to the creep index n of the material for minimum creep rates.

In the second approach, used by Webster (1975), Landes & Begley (1976) and Harper & Ellison (1977), it is suggested that the rate of crack growth depends on C^* a parameter derived from J by replacing strain and displacement by strain-rate and displacement-rate.

In the third approach, described by Neate (1977), the component lifetimes are determined by using either a representative rupture stress or the average stress which acts on the minimum section of the crack plane. This technique was first identified, for simple plate structures, by Hayhurst (1973), Hayhurst *et al.* (1975 *a*, *b*), and for axisymmetrically notched bars by Hayhurst *et al.* (1978); in addition, its application to structures that contain sharp cracks has been done by Leckie & Hayhurst (1981). The technique reflects the ability of a structure to redistribute stress away from regions of stress concentration and to behave as a body subjected to relatively uniform states of multi-axial stress.

A difficulty encountered in the use of these theories in component design is the identification of the appropriate calculation for a particular material and the structural component in question. A better understanding of this situation has been provided by Riedel (1978), Riedel & Rice (1980), Hui & Riedel (1981) who considered the characterization of crack tip fields in elastic-nonlinear viscous materials and so were able to identify the régimes in which the different parameters are appropriate. Ainsworth (1982) has examined the equations for the steady-state motion of a crack in a creeping structure and has shown that, for certain crack velocities, it is unnecessary to obtain general solutions for the equations. Instead, the solutions may be described by K and J for steady-state. The selection of the appropriate parameter is dependent on the value of n and on a normalized crack velocity. Unfortunately there is an intermediate range of crack velocities for which neither K nor J is appropriate. The range of validity of K has been shown to be limited to materials with low n and high crack velocities. The range of validity of J is broader, and it is appropriate for materials having high n values and low crack velocities. For materials that exhibit pronounced tertiary creep, crack velocities may be sufficiently low for lifetimes to be predicted directly from a representative rupture stress. Ainsworth (1982) has defined the range of crack velocities for which each of the three mechanisms may be expected to be appropriate.

Of the theories described so far only the representative rupture stress theory is based upon physically realistic mechanisms (Hayhurst *et al.* 1984). The techniques that make use of K and J are *ad hoc* extensions of classical fracture theories from temperatures below the creep range to temperatures above it. Such extensions have not been justified by consideration of the physical processes which operate in the creep range. This is the principal deficiency of these techniques since the purpose of developing such theories is to extrapolate short-term laboratory data, obtained from small specimens, to larger structural components which are to operate for

2×10^5 h. The only characteristic that can be used to justify extrapolation is that the same physical mechanisms operate in the short term, in the laboratory, as operate in the long term, in the real structure. The same point has been made by Ashby (1972) in the context of the extrapolation of short term uni-axial data to long term applications. It is imperative, therefore, that further developments of these theories be related to the governing physical mechanisms.

(*c*) *Physical mechanisms of crack growth*

The physical processes by which materials degenerate and rupture because of exposure to stress at high temperatures have been discussed by Ashby (1972) and by Dyson (1978). Materials fail by the nucleation and the growth of grain boundary defects by mechanisms appropriate to the operating temperature, stress level and stress state. The time-dependent processes by which grain boundary defects nucleate are not well understood (Raj & Ashby 1975; Hayhurst *et al.* 1980, 1983). In comparison, the processes by which grain boundary defects grow are well understood and they have been reviewed by Cocks & Ashby (1982*a*) and by Dyson (1976, 1978). At high overall stresses the growth of grain boundary defects is controlled by power-law creep of the bulk of the material; the mechanism is similar to that responsible for time-independent void growth at low temperatures and results in short lifetimes. At medium stress levels, the lifetimes are long, typically 10^4–10^5 h, the ductility is lower and the growth of defects is caused by diffusion. Voids grow and link up to produce grain boundary cracks before extensive creep of the bulk of the material takes place. Recent work by Dyson (1978) has shown that for appropriately low levels of overall stress the void growth rate is constrained by the creep deformation of the surrounding grains. These mechanisms are thought to operate in crack-tip situations; however, a criticism that may be levelled is that, with the exception of the work on power law creep by Cocks & Ashby (1982*a*), the theories have been derived for one-dimensional states of stress, which are not encountered in the fracture process zones ahead of plane strain cracks. Of additional concern is the paucity of creep rupture data for materials subjected to the multi-axial states of stress found at the tips of sharp cracks; the work of Dyson & Loveday (1981) and of Needham & Gladman (1980) being notable exceptions. An equally valid criticism is that most physical metallurgical theories do not take account of the effects of grain boundary damage on the strain rate processes. This is an important omission since it results in significant time dependent stress redistribution (Hayhurst 1973) which can have a pronounced influence on component lifetimes. The limitations of conventional physical metallurgical theories in modelling the interactions between material behaviour on the one hand and the performance of structural components on the other have been discussed by Hayhurst *et al.* (1975*a*). They used a single state damage variable theory which has been shown by Leckie & Hayhurst (1977) and by Cocks & Ashby (1982*a*) to be consistent with the physical metallurgical theories for proportional loading; its main advantage is that it is flexible and simple to use in the solution of boundary value problems. The use of the single state damage variable theory in the solution of creep crack growth problems will be discussed in a later section.

(*d*) *Estimation of crack growth rates by using crack-tip fields and void growth rate equations*

Constitutive equations, for the growth of grain boundary defects, have been used to study the growth of cracks in structural members; the results of such investigations will now be discussed. Riedel (1981) has used the crack-tip stress fields, due to Hutchinson (1968) and to Rice & Rosengren (1968) and known as the H.R.R. fields, in conjunction with material models that describe

PHILOSOPHICAL TRANSACTIONS OF THE ROYAL SOCIETY A MATHEMATICAL, PHYSICAL & ENGINEERING SCIENCES

void growth by power law creep and by vacancy diffusion. Crack advance is assumed to occur when damage, defined at a distance X_c ahead of the crack, reaches a critical value. The material models assume that the growth of damage is determined by stress, although in the case of power law creep the criterion is equivalent to a critical strain criterion. The results of the study identify the conditions in which each material mechanism operates; in addition, the theoretical predictions were compatible with the results of experiments carried out on 304 stainless steel. Cocks & Ashby (1982*b*) have adopted a similar approach to that used by Riedel (1981) except that their formulation is expressed in terms of the H.R.R.-strain rate field and that use is made of a critical value of the effective strain as the failure criterion, at a defined point ahead of the crack-tip. For void growth by power law creep the two approaches give similar results, but for the diffusion controlled growth mechanism the predictions of the two approaches differ. The theory due to Cocks & Ashby (1982*b*) was shown to predict the results of tests carried out by Taira *et al.* (1979) on thin tubular specimens. Ohtani (1981) used a similar approach to Riedel (1981) and to Cocks & Ashby (1982*b*), but, instead of using the H.R.R. fields he used a finite deformation, finite element, technique coupled with a limiting effective strain failure criterion in a power law, non-damaging, creeping material. He showed that the relation between the *J*-integral and the near-tip creep rates was the same for both the propagating and the stationary crack. The results of experiments correlated well with the *J*-integral. It was found that the effects of finite deformations may be corrected for by taking into consideration the reduction in specimen width. Hutchinson (1983) has used a constitutive equation, for a material undergoing grain boundary cavitation, in which the strain rates are uniquely defined by the degree of cavitation, stress and stress state, to obtain crack-tip stress fields in a region of uniform cavitation; they are similar to the H.R.R. fields for undamaged material. The solutions show that the dilatation rates determined by using the H.R.R. fields substantially overestimate the dilatation rate, determined from the damage model. Hutchinson's work does not include a study of a moving crack. Leckie & Hayhurst (1981) have described the effects of stress state on the strain to failure by using a single state variable damage theory for copper. The resulting expression has been used together with results from McMeeking (1977) for the stress and strain fields, caused by finite deformations at the crack tip, to determine the location, in front of the crack, and the magnitudes of stress and strain required for local failure. When this condition is satisfied the material in the region between the crack tip and the point of failure is assumed to rupture and the crack to advance to the failure point. The procedure is repeated until the crack reaches its critical length and failure takes place. The theory predicts a crack advance which is so slow that failure in copper occurs first by continuum damage mechanics.

A degree of commonality exists between the theories described above and that will now be discussed. With the exception of the work of Riedel and his collaborators and of Ohtani (1981) none of the theories includes the effects of elasticity during crack propagation; this can be of importance in situations where timescales for stress redistribution are long. With the possible exception of the work by Leckie & Hayhurst (1981) the multi-axial stress rupture behaviour of the materials is inappropriately modelled for crack-tip situations: most of the material models pertain to, and have been checked against data for, uni-axial situations. None of the models discussed above describes the effects of continuum damage, or tertiary creep, on regions well removed from the crack. This is of importance since in realistic design situations the timescales are sufficiently long for the continuum to damage and to result in significant stress redistribution. If the importance of such features is to be assessed then it is necessary to carry out a full elastic-creep solution of the boundary value problem which allows primary, secondary and tertiary

PHILOSOPHICAL TRANSACTIONS OF THE ROYAL SOCIETY A MATHEMATICAL, PHYSICAL & ENGINEERING SCIENCES

creep in addition to permitting the growth of single creep cracks. The possibility of this type of solution is now discussed.

(*e*) *Present investigation*

In an earlier paper Hayhurst *et al.* (1984) have studied the creep rupture of two axi-symmetrically notched bars. One is a circular notched bar studied by Bridgman (1952), which is subjected to relatively homogeneous states of stress, and the other is the British Standard (1969) *v*-notched bar, which has a high stress concentration factor and is subjected to non-uniform stress distributions. The study involved the use of the finite element method to solve the elastic and creep problems; the technique is based on the theory of continuum damage mechanics and requires the use of constitutive equations to describe the entire creep strain and damage processes under multi-axial states of stress. The method allows creep damage to grow and the boundary value problem to be redefined, when local failure occurs. In this way the advancement of a zone of damage or a crack may be modelled. The results of the investigation showed that for the circular notch the initial stress concentrations were nullified and damage formed in a reasonably uniform way across the minimum section of the notch. Failure took place in a manner similar to that for a homogeneously stressed material. For the B.S. notch the character of the initial stress concentration persisted and the damage developed in a non-uniform way. The region of pronounced growth was very confined and crack-like in character, but regions of lower damage were observed throughout the body. That observation is of interest since it implies that creep crack growth takes place by the growth of continuum damage which is confined, by the character of the stress field, to a narrow crack-like region. In this paper the assumption will be made that the growth of cracks by creep can be modelled by using continuum damage mechanics; the numerical procedures previously developed by Hayhurst *et al.* (1984) will be used to study the creep crack growth behaviour of the specimen geometries reported by Hayhurst *et al.* (1981). The theoretical results will be compared with the results of experiments and with metallographic studies carried out on cracked specimens close to failure; creep damage and stress fields for both specimens will be presented and the time variation of spatial distributions of stress and strain will be discussed for the minimum section.

2. Experimental programme

(*a*) *Plane strain specimen design*

Symmetrically cracked tension specimens have been selected to avoid the bending stresses associated with asymmetrically cracked tension specimens and to avoid the large deformations which result. Internally and externally cracked specimens were chosen with the geometries defined in figure 1 and in table 1 and were subjected to the boundary stress σ_0; these geometries are identical to the notch type 1 geometries reported by Hayhurst *et al.* (1981). These specimens were selected to vary the degree of the tri-axial tension stress invariant, J_1 ($= \sigma_{ii}$), ahead of the crack. From the perfect plasticity solutions of Ewing & Hill (1967) it is known that the double edged cracked specimen generates high positive values of J_1. The values of $a/b = \frac{1}{8}$, for internally cracked specimens, and $a/b = \frac{2}{3}$, for externally cracked specimens, were selected for the same reason. Plane strain conditions were achieved by making the specimen thickness, W, large compared with the crack length, a.

(*b*) *Selection of materials*

The three materials selected are those used by Hayhurst *et al.* (1984). The aluminium alloy and the 316 stainless steel specimens were manufactured from the same ingot but the copper specimens were manufactured from a different extruded bar. The materials were selected since they represent extreme types of multi-axial stress rupture behaviour. The aluminium alloy ruptures according to a maximum effective stress σ_e ($= (\frac{2}{3}S_{ij}S_{ij})^{\frac{1}{2}}$, where S_{ij} is the stress deviator given by $S_{ij} = \sigma_{ij} - \frac{1}{3}\delta_{ij}\sigma_{kk}$) and the copper and 316 stainless steel rupture according to mixed criteria, which are predominantly maximum principal tension stress, σ_1, dependent. The tests were done on the cracked specimens under steady load and at temperatures of 210 ± 1 °C for the aluminium alloy specimens, 250 ± 1 °C for the copper specimens and at 550 ± 2 °C for the 316 stainless steel specimens.

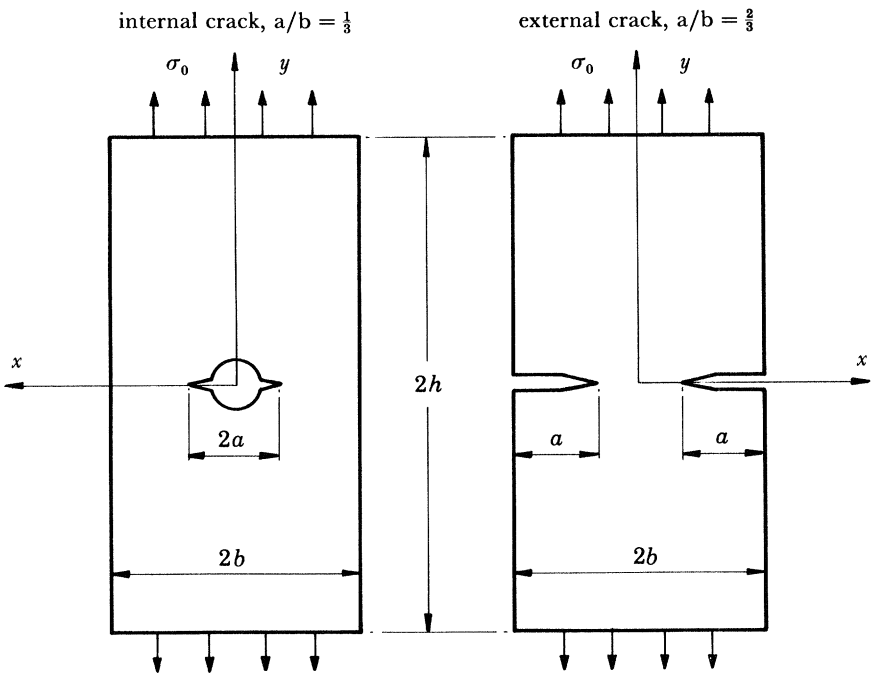

FIGURE 1. Definition of coordinate system for internally and externally cracked specimens.

TABLE 1. SPECIMEN DIMENSIONS IN MILLIMETRES; W IS THE SPECIMEN THICKNESS

dimension	internal crack $a/b = \frac{1}{3}$	external crack $a/b = \frac{2}{3}$
a	4.19	6.35
b	12.70	9.53
W	22.23	38.10
h	30.16	36.51

(*c*) *Experimental results*

Graphs of the average stress acting on the minimum section, σ_N ($= P/2(b-a)$), where P is the applied tension load, against component lifetime have been presented by Hayhurst *et al.* (1981) for the copper and the stainless steel specimens; the experimental results reported there for an aluminium alloy, referred to as D19S, have not been used in this paper. Instead the

aluminium alloy reported by Hayhurst *et al.* (1975 *a*) has been used since the constitutive equations have already been developed for that material. The uni-axial rupture data for this material have been reproduced in figure 2 together with the test results for internally and externally cracked specimens. The experimental results, presented in these graphs, will be discussed in terms of the representative rupture stress used by Hayhurst *et al.* (1978). The performance of cracked members may be expressed in terms of the applied average stress, σ_n, compared with the stress, σ_r, in parallel sided uni-axial creep specimen which has the same lifetime as the

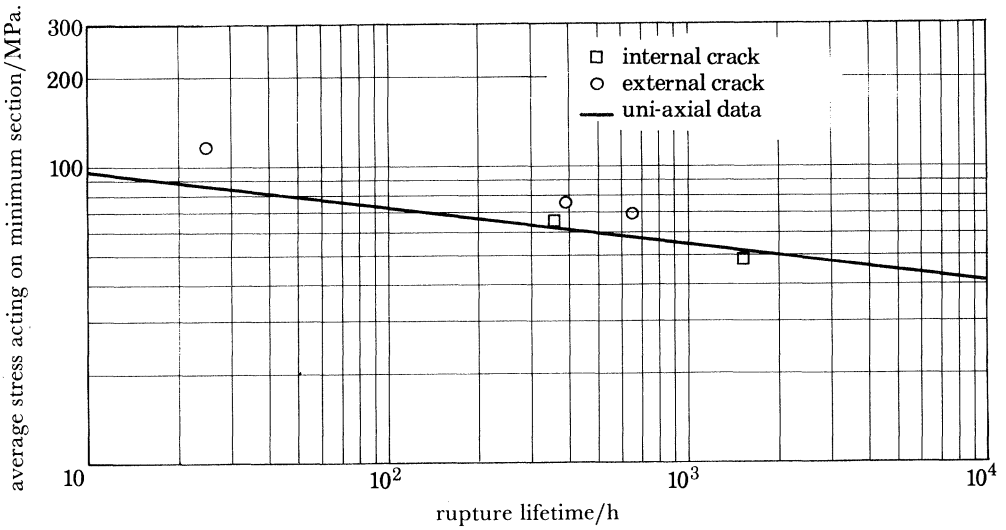

FIGURE 2. Comparison of lifetimes for plane strain internally and externally cracked specimens with uni-axial data for the aluminium alloy tested at 210 °C.

TABLE 2. EXPERIMENTAL VALUES OF THE NORMALIZED REPRESENTATIVE RUPTURES STRESS FOR BOTH SPECIMEN GEOMETRIES AND A COMPARISON OF THEIR RATIOS WITH THEORETICALLY DETERMINED VALUES

	experimental representative rupture stress		$\Sigma_r^{int}/\Sigma_r^{ext} = (\sigma_n^{ext}/\sigma_n^{int})_{t_f = \text{constant}}$		
material	internal crack Σ_r^{int}	external crack Σ_r^{ext}	experiment	$\dot{a} \propto K_I^s(a/b)$ (1*a*)	$\dot{a} \propto J(t, a/b)$ (1*b*)
aluminium alloy	1.00	0.78	1.28	1.38	1.46
copper	1.01	0.87	1.16	1.07	1.15
316 stainless steel	1.25	0.93	1.34	1.16	1.27

cracked bar. The normalized representative rupture stress Σ_r is defined by σ_r/σ_n. A specimen which requires a lower uni-axial stress σ_r, than the average stress σ_n is said to be notch strengthening ($\Sigma_r < 1$) and, conversely a specimen which requires a higher uni-axial stress σ_r than the average stress σ_n is said to be notch weakening ($\Sigma_r > 1$). Experimental values of Σ_r for internally and externally cracked specimens are given in table 2. Corrections have been made to take account of stress changes during deformation in both the cracked and uni-axial tests. The corrections were made using the method described by Hayhurst *et al.* (1978) for notched bars. The values of Σ_r show a decreasing level of strengthening for the externally cracked members and an increasing level of weakening for the internally cracked members for the aluminium alloy, the copper and the 316 stainless steel respectively.

3. Lifetimes determined from K and J

The experimental results for the copper and 316 stainless steel specimens have been presented by Hayhurst *et al.* (1981) together with results for a different aluminium alloy, D19S. The representative rupture stresses are similar for the D19S material and for the aluminium alloy reported here; the values for the externally and internally cracked specimens are respectively: 0.80 and 1.00, for D19S and 0.78 and 1.00, for the other material. The purpose of the investigations carried out by Hayhurst *et al.* (1981) was to investigate the accuracy with which the following relations,

$$\mathrm{d}a/\mathrm{d}t \propto (K_{\mathrm{I}}(a/b))^{S}, \tag{1a}$$

and

$$\mathrm{d}a/\mathrm{d}t \propto J(t, a/b), \tag{1b}$$

can predict the lifetimes of the internally and externally cracked specimens. The use of the two geometries enabled the constant of proportionality in (1) to be eliminated. The values of J, obtained by Hayhurst & Brown (1984), were described as a function of a/b by using a cubic spline function, and the values of K_{I} were described as a function of a/b by using functional representations given in data books (Tada *et al.* 1973). Equations (1) were then integrated with these functional representations to obtain values of $(\Sigma_{\mathrm{r}}^{\mathrm{int}}/\Sigma_{\mathrm{r}}^{\mathrm{ext}})$, where $\Sigma_{\mathrm{r}}^{\mathrm{int}}$ and $\Sigma_{\mathrm{r}}^{\mathrm{ext}}$ are the normalized representative rupture stresses of the internally and externally cracked specimens respectively. The correlations between theory and experiment, given in table 2, were made with $S = n$, where n is the stress index for minimum creep rates. The ratio $(\Sigma_{\mathrm{r}}^{\mathrm{int}}/\Sigma_{\mathrm{r}}^{\mathrm{ext}})$ may be shown to equal the ratio $(\sigma_{\mathrm{r}}^{\mathrm{ext}}/\sigma_{\mathrm{r}}^{\mathrm{int}})$, when both specimens have the same lifetime t_{f}. For the aluminium alloy, D19S, the predictions are that an externally cracked specimen is 38 % stronger than an internally cracked specimen, with the same lifetime, for (1*a*) and 46 % stronger for (1*b*); these are, respectively, 10 % and 18 % higher, in terms of stress, than the corresponding experimental result. In the case of copper the predictions are that an externally cracked specimen is 7 % stronger than an internally cracked specimen for (1*a*), 15 % for (1*b*), and 16 % in the case of the experimental result. For the 316 stainless steel material the predictions are that an externally cracked specimen is 16 % stronger than an internally cracked specimen for (1*a*), 27 % for (1*b*), and 34 % for the experimental result. The poor agreement between theory and experiment in the case of aluminium is not surprising since the cracks did not propagate in the plane of the original crack but in a plane inclined at approximately 55° to it, as shown in figure 3, plate 1, for the externally cracked specimen in the D19S alloy. Failure may be observed from the figure to have taken place due to a shear controlled void growth mechanism. The predictions for the copper and for the 316 stainless steel specimens made by using (1*b*) are probably sufficiently accurate for the purposes of engineering design. However, the prediction methods based on (1) do not reflect the governing physical processes; for this reason they do not identify those conditions for which the crack growth takes place in planes different from the initial crack plane. In the next section a numerical solution procedure for the creep rupture of cracked members, based on continuum damage mechanics, will be described in which the controlling physical processes are more realistically modelled.

4. Theoretical investigation

(*a*) *Numerical procedure*

The numerical procedure used to solve the boundary value problem is that used by Hayhurst *et al.* (1984). It is based on the finite element method and employs constant strain triangular

elements; the singular crack-tip fields encountered in the solution of stationary-state creep problems have been modelled (Hayhurst & Brown 1984) by using this class of element, and the resulting values of the J contour integral were shown to be in close agreement with existing results obtained with crack-tip elements with singular displacement fields. Finite element meshes similar to those used by Hayhurst & Brown (1984) have been used here. The solution method is based upon the theory of continuum damage mechanics which allows damage to initiate and to grow throughout the body as a field quantity. The procedure takes the elastic solution as its starting point and integrates creep strain, stress and creep damage with respect to time. The integration is carried out over a series of discrete time steps using a fourth-order Runge–Kutta technique; this procedure involves the repeated solution of the boundary value problem to determine the field quantities required for the numerical integration. Creep damage, as represented by a single damage state variable, develops monotonically in time throughout the structure, and failure of an element is deemed to have occurred when the state parameter attains a prescribed value. The material element is then unable to transmit or sustain load and it is removed from the model; so that the boundary value problem is redefined, which permits either a crack to develop or a zone of failed material to spread out. Once the boundary value problem is redefined the time integration is continued taking the field variables, before the local failure occurred, as the new starting point. The procedure is then repeated until complete failure of the cracked member occurs. The use of this method to study sharp crack problems may be justified since Hayhurst *et al.* (1984) have shown that for v-notched tension bars, where high stress gradients are found, single crack-like behaviour is well modelled.

(*b*) *Constitutive equations*

The development of a constitutive equation for multi-axial creep strain rates has been discussed by Hayhurst *et al.* (1984); the equation is given by

$$\dot{v}_{ij} = G(1-\omega)^{-n} t^m \partial[\Psi^{n+1}(\sigma_{kl})/(n+1)]/\partial\sigma_{ij}, \tag{2}$$

where G, n and m are material constants used to fit (2) to experimental data; n need not be the stress index for minimum creep rates. On introduction of the normalized parameters

$$\Sigma_{ij} = \sigma_{ij}/\sigma_0, \quad V_{ij} = v_{ij}/e_0,$$

$$\lambda_{ij} = \epsilon_{ij}/e_0 \quad \text{and} \quad \tau = \int_0^t GE\sigma_0^{(n-1)} t^m \mathrm{d}t,$$

where λ_{ij} is the normalized total strain tensor, e_0 is the uni-axial elastic strain given by σ_0/E, E is Young's modulus and τ is a normalized measure of time, then (2) can be rewritten as

$$\dot{V}_{ij} = \mathrm{d}V_{ij}/\mathrm{d}\tau = (1-\omega)^{-n} \partial[\Psi^{n+1}(\Sigma_{kl})/(n+1)]/\partial\Sigma_{ij}. \tag{3}$$

When $\omega = 0$ the material is in its virgin state and Norton's law is recovered from (3), when $\omega = 1$ the creep strain rates are infinite and the material is at failure. The evolution equation for the damage state variable has been discussed by Hayhurst *et al.* (1984) and is given by

$$\dot{\omega} = M[\alpha\sigma_1 + (1-\alpha)\sigma_e]^\chi t^m/[(1+\phi)(1-\omega)^\phi], \tag{4}$$

where M, α, and ϕ are material constants. This equation represents a multi-axial generalization of the theories due to Kachanov (1960) and to Rabotnov (1969). Equation (4) may be normalized by using the quantities defined above and rewritten as

$$\dot{\omega} = \mathrm{d}\omega/\mathrm{d}\tau = [\alpha\Sigma_1 + (1-\alpha)\Sigma_e]^\chi/[V_u(1+\phi)(1-\omega)^\phi], \tag{5}$$

where $V_u = (GE/M)\,\sigma_0^{(n-\chi-1)}$. Integration of (5) with the limits $\omega = 0$, $\tau = 0$ and $\omega = 1$, $\tau = \tau_f$ yields an expression for the rupture lifetime for a given stress state. The expression obtained may be normalized to give the equation of the isochronous locus in stress space. Such loci have been presented by Hayhurst (1972) and by Hayhurst *et al.* (1984) for a range of materials in principal plane stress space. The parameter α, in (5), determines the form of the isochronous locus; $\alpha = 0$ represents a maximum effective stress rupture criterion and $\alpha = 1$ represents a maximum principal tension stress rupture criterion.

To determine the material constants it is necessary to carry out uni-axial tests to define the parameters in (3) and (5), but before α can be determined it is necessary to carry out tests under two different stress states. Test procedures for carrying this out have been suggested by Hayhurst *et al.* (1984). Some of the data for the aluminium alloy and for the 316 stainless steel have been presented by Hayhurst *et al.* (1984) and are summarized in table 3. Uni-axial data for the new extruded copper bar used in the work reported here are presented in figure 4, where they are compared with values of strain computed by using the uni-axial form of (2), the corresponding data being given in table 3.

TABLE 3. SUMMARY OF MATERIAL CONSTANTS EXPRESSED IN UNITS OF MEGAPASCALS, PERCENTAGE CREEP STRAIN AND HOURS

parameter	aluminium alloy	copper	316 stainless steel
E/MPa	60.03×10^3	66.24×10^3	169.617×10^3
ν	0.30	0.30	0.300
n	6.90	2.97	1.737
m	−0.20	−0.79	−0.940
χ	6.48	1.21	0.478
ϕ	9.50	3.83	1.914
α	0	0.70	0.750
G	1.15×10^{-15}	1.28×10^{-6}	1.383×10^{-5}
M	1.79×10^{-14}	6.02×10^{-4}	2.774×10^{-3}
$\hat{\sigma}$	—	—	441.28
χ_A	—	—	4.00

In studies of the behaviour of sharp cracks the crack-tip regions are inevitably subjected to high stresses and it is necessary to examine the short term behaviour for stresses close to yield. The effect of high stresses is often reflected by a change in slope of the graph of logarithm (applied uni-axial stress) against logarithm (lifetime), at stresses close to yield. A similar effect can often be observed in the graph of $\ln \sigma$ against $\ln \dot{v}_{\min}$. In the cases of the aluminium alloy and of copper both graphs remain linear even for very short-term behaviour. For stainless steel there is a marked change of slope in the graph of $\ln t_f$ against $\ln \sigma$ at the stress $\hat{\sigma} = 441.28$ MPa. This behaviour is shown in figure 5; for stresses in excess of $\hat{\sigma}$ the time-independent strains on loading were large relative to the creep strains and the values of stress have been corrected for initial geometry changes. Values of stress less than $\hat{\sigma}$ have been plotted in figure 5 on a nominal stress basis. The uni-axial strain rate data for 316 stainless steel, when plotted on the axes $\ln \sigma$ against $\ln \dot{v}_{\min}$, is closely approximated by a straight line. The bilinear rupture curve shown in figure 5, requires (4) to be modified; it is necessary to use two equations, one for each portion of the graph. Two values of C and χ have to be defined, C_A, χ_A for $\sigma > \hat{\sigma}$ and C, χ, for $\sigma \leqslant \hat{\sigma}$, the values of m, α, ϕ and V_u are assumed to be constant. On integration of (4) for the initial and the final conditions

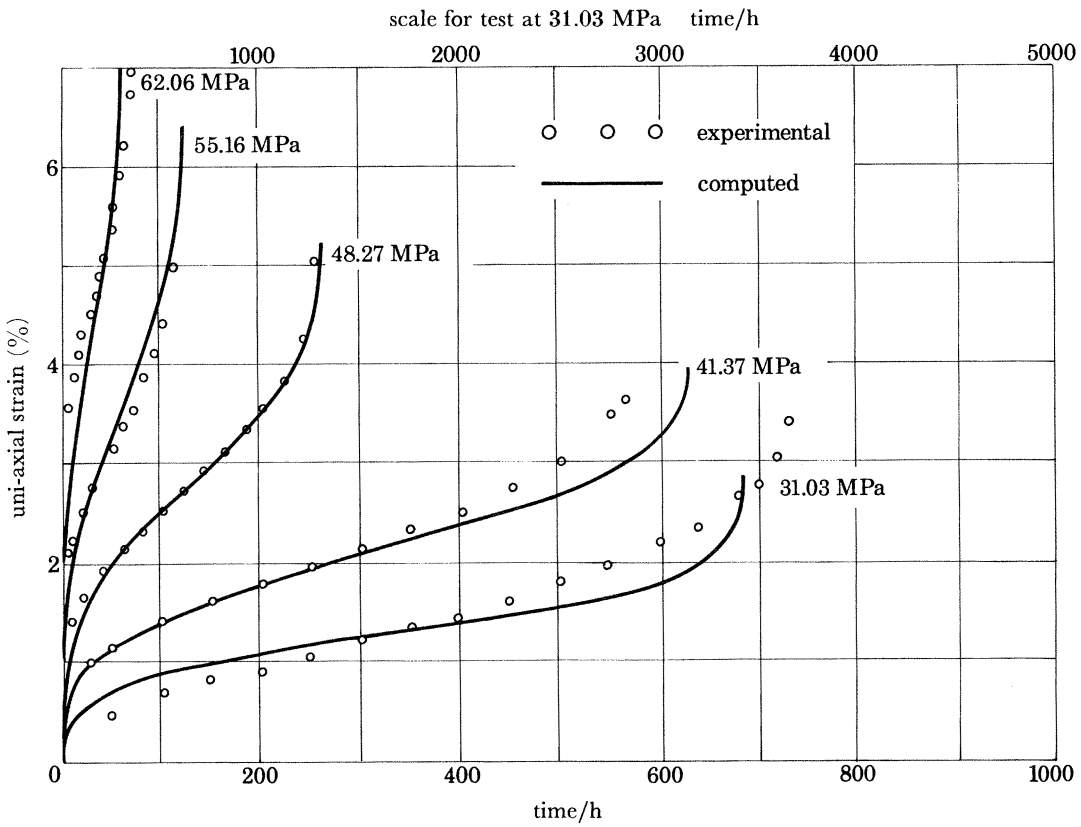

FIGURE 4. Comparison of computed with experimental values of strain for copper tested at 250 °C.

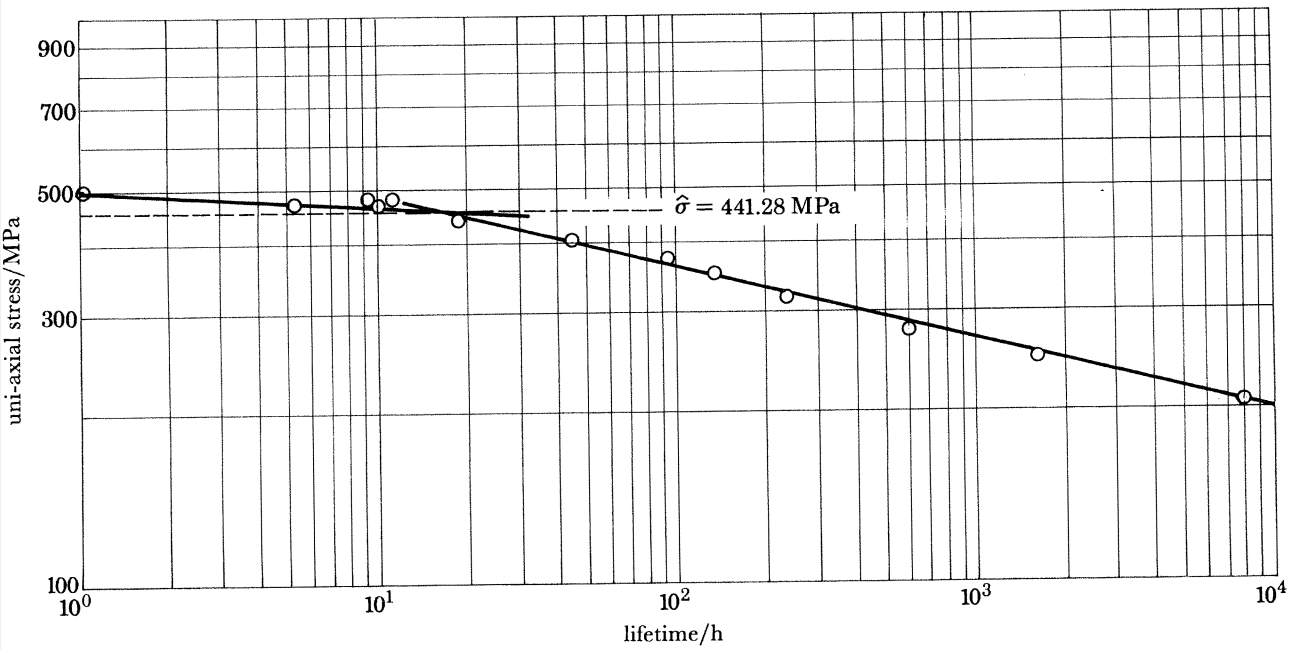

FIGURE 5. Uni-axial rupture data for 316 stainless steel at 550 °C.

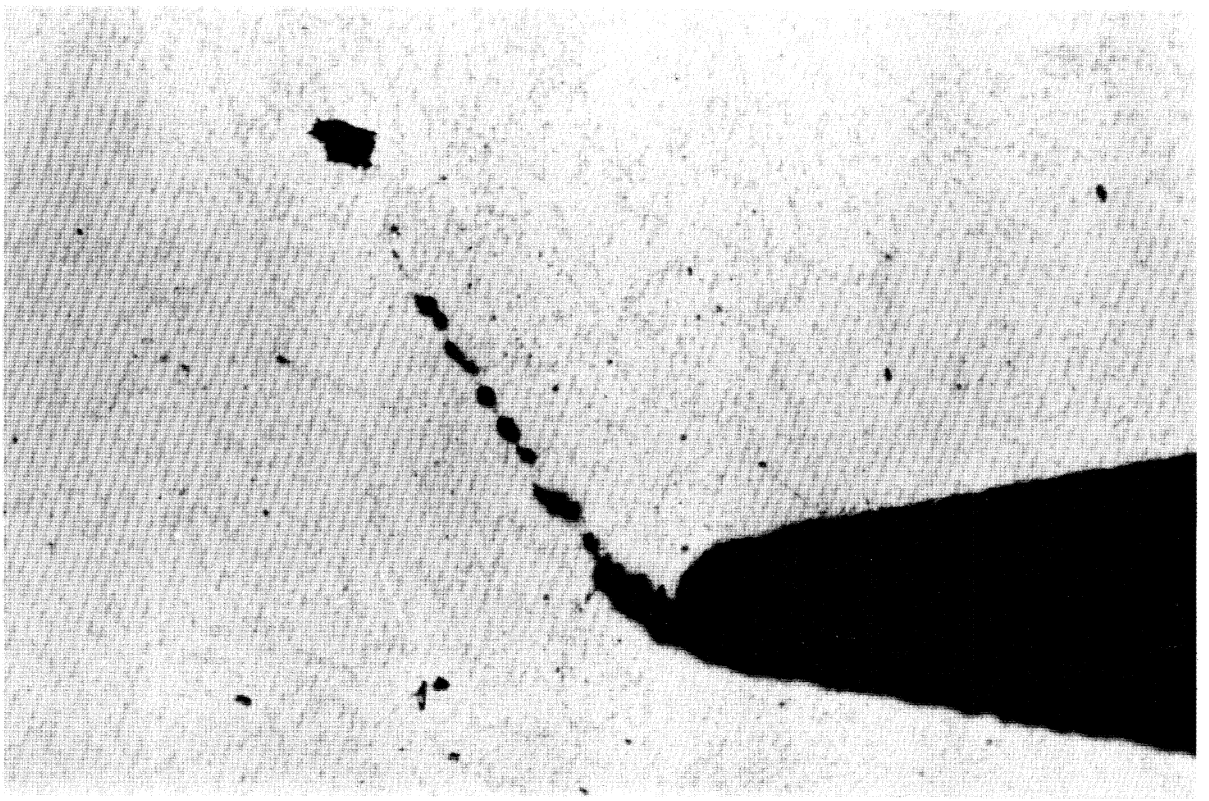

FIGURE 3. Crack tip shear damage, close to failure, in an externally cracked specimen made from D19S aluminium alloy and tested at 150 °C (magnification × 90).

(*Facing p.* 142)

PHILOSOPHICAL TRANSACTIONS OF THE ROYAL SOCIETY A MATHEMATICAL, PHYSICAL & ENGINEERING SCIENCES

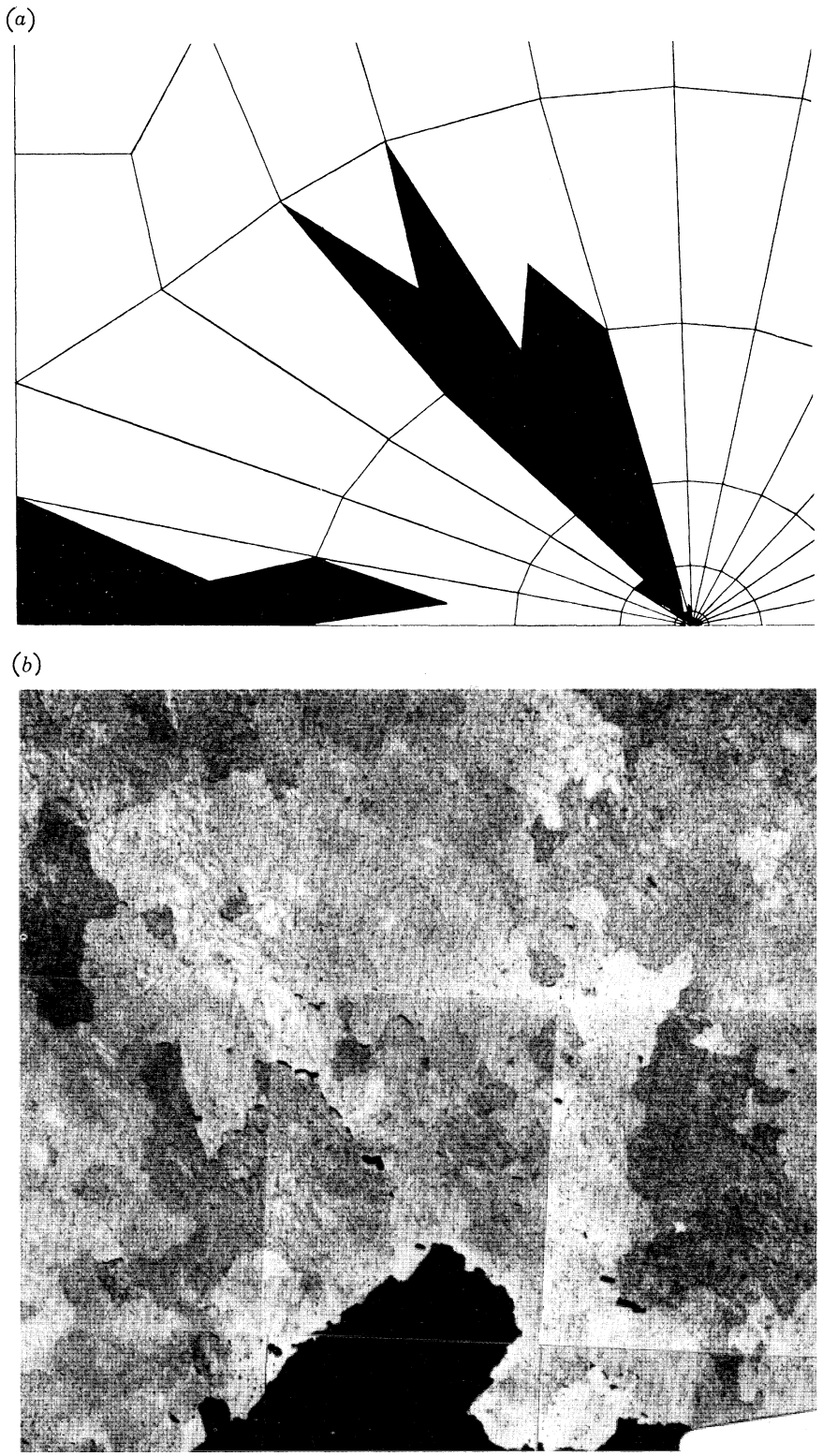

FIGURE 6. Comparison of (*a*) computed failure path, $\omega \geqslant 0.999$, with (*b*) mid-thickness micrograph taken from the minimum section of an externally cracked specimen in an aluminium alloy at failure. Original crack profile shown in white.

PHILOSOPHICAL TRANSACTIONS OF THE ROYAL SOCIETY A MATHEMATICAL, PHYSICAL & ENGINEERING SCIENCES

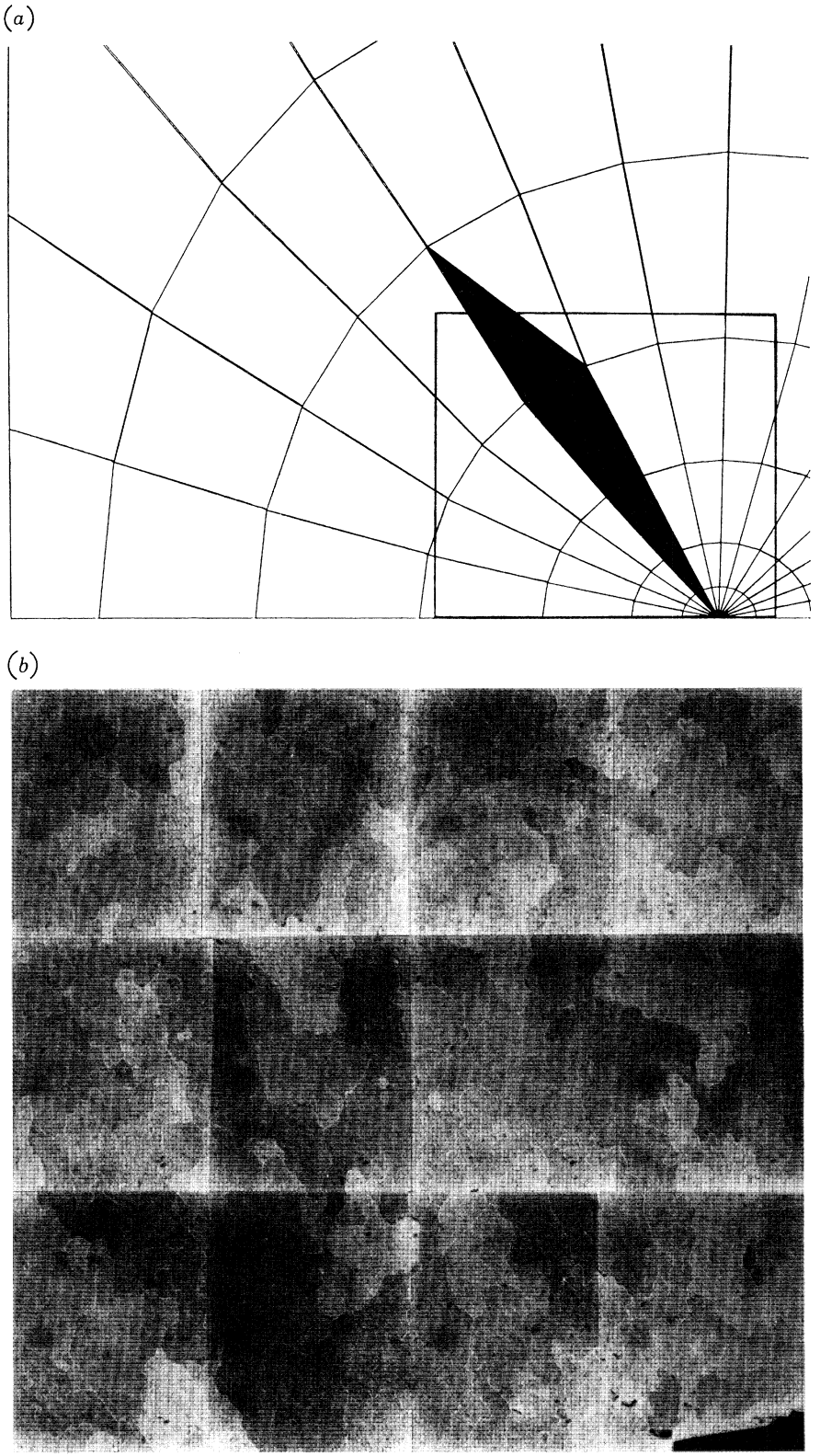

FIGURE 7. Comparison of (*a*) computed failure path, $\omega \geqslant 0.999$, for the minimum section with (*b*) a mid-thickness micrograph taken from a selected region of an internally cracked specimen in an aluminium alloy at $t/t_t = 0.95$.

PHILOSOPHICAL TRANSACTIONS OF THE ROYAL SOCIETY A MATHEMATICAL, PHYSICAL & ENGINEERING SCIENCES

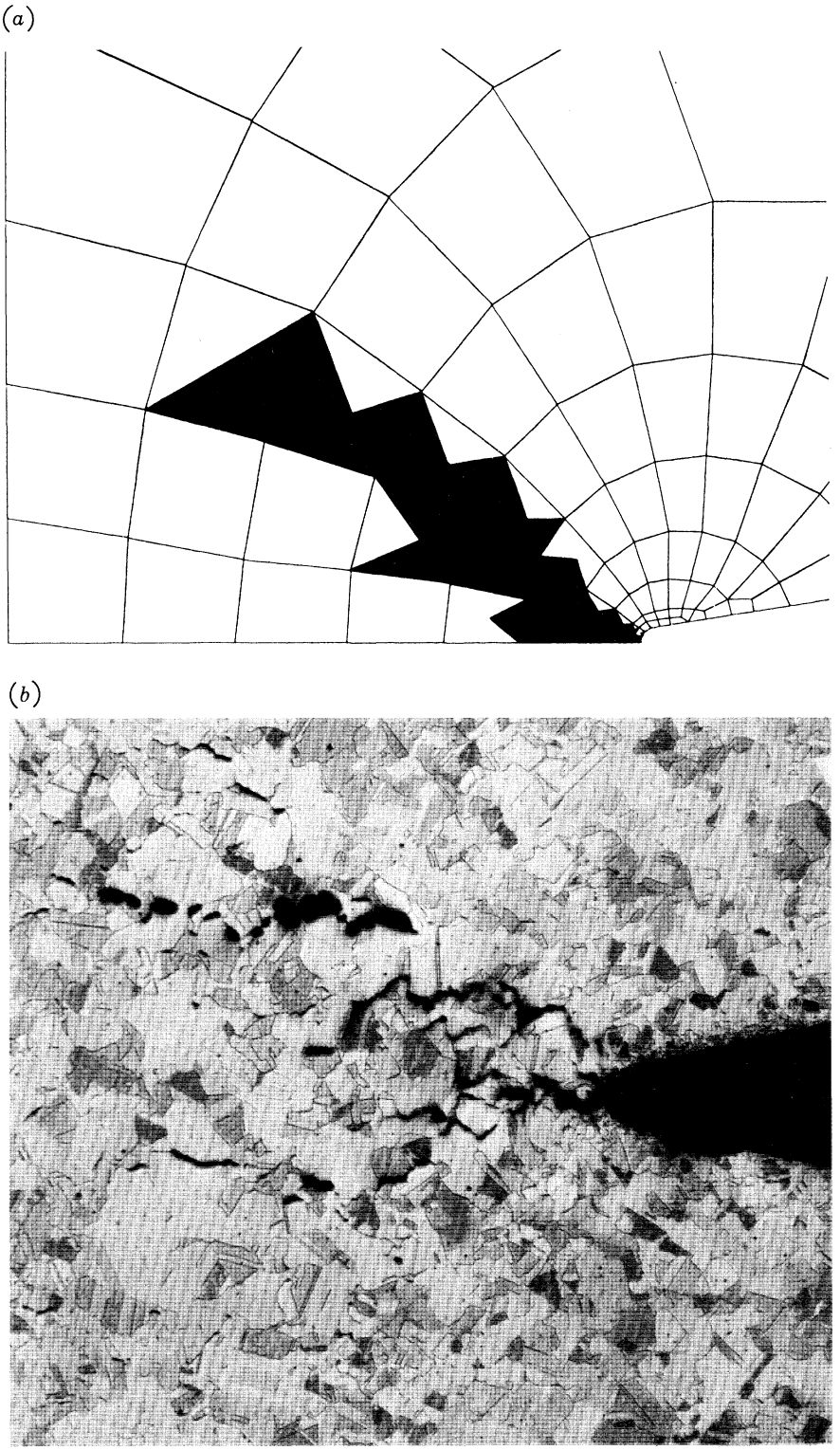

FIGURE 11. Comparison of (*a*) computed failure path, $\omega \geqslant 0.999$, with (*b*) mid-thickness micrograph taken from the minimum section of an externally cracked specimen in copper at $t/t_f = 0.94$.

PHILOSOPHICAL TRANSACTIONS OF THE ROYAL SOCIETY A MATHEMATICAL, PHYSICAL & ENGINEERING SCIENCES

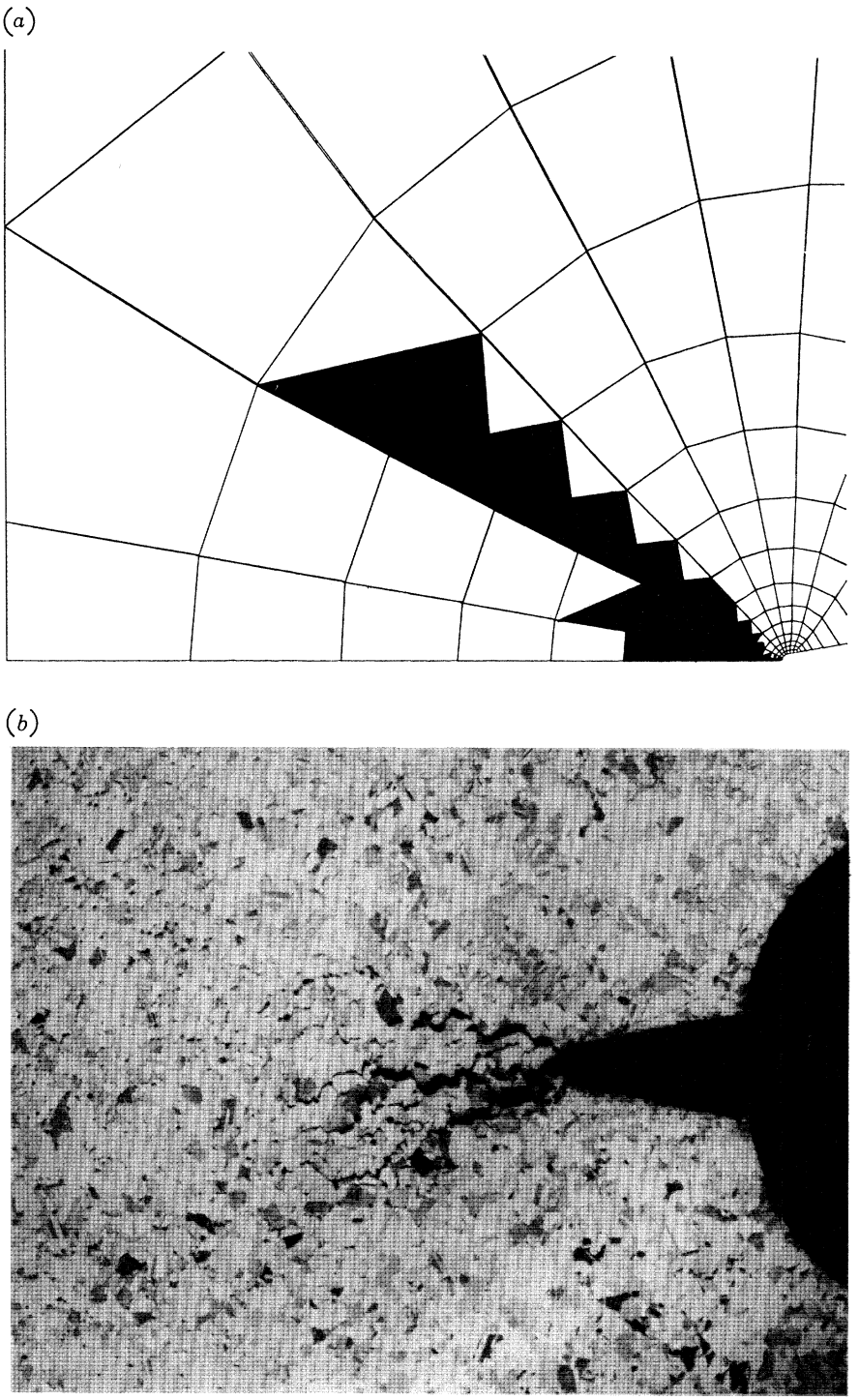

FIGURE 12. Comparison of (*a*) computed failure path, $\omega \geqslant 0.999$, with (*b*) mid-thickness micrograph taken from the minimum section of an internally cracked specimen in copper at $t/t_t = 0.99$.

PHILOSOPHICAL TRANSACTIONS OF THE ROYAL SOCIETY A MATHEMATICAL, PHYSICAL & ENGINEERING SCIENCES

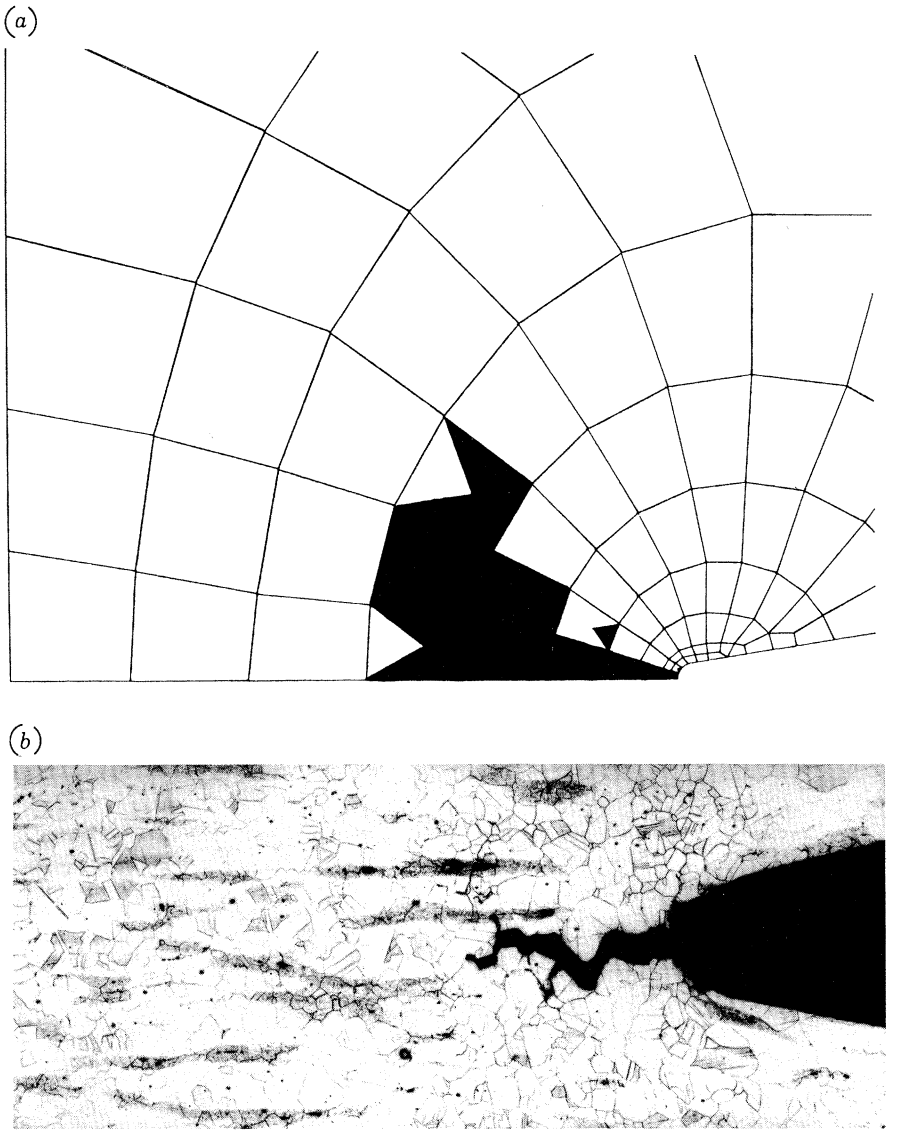

FIGURE 16. Comparison of (*a*) computed failure path, $\omega \geqslant 0.999$, with (*b*) mid-thickness micrograph taken from the minimum section of an externally cracked specimen in 316 stainless steel at $t/t_t = 0.6$.

PHILOSOPHICAL TRANSACTIONS OF THE ROYAL SOCIETY A MATHEMATICAL, PHYSICAL & ENGINEERING SCIENCES

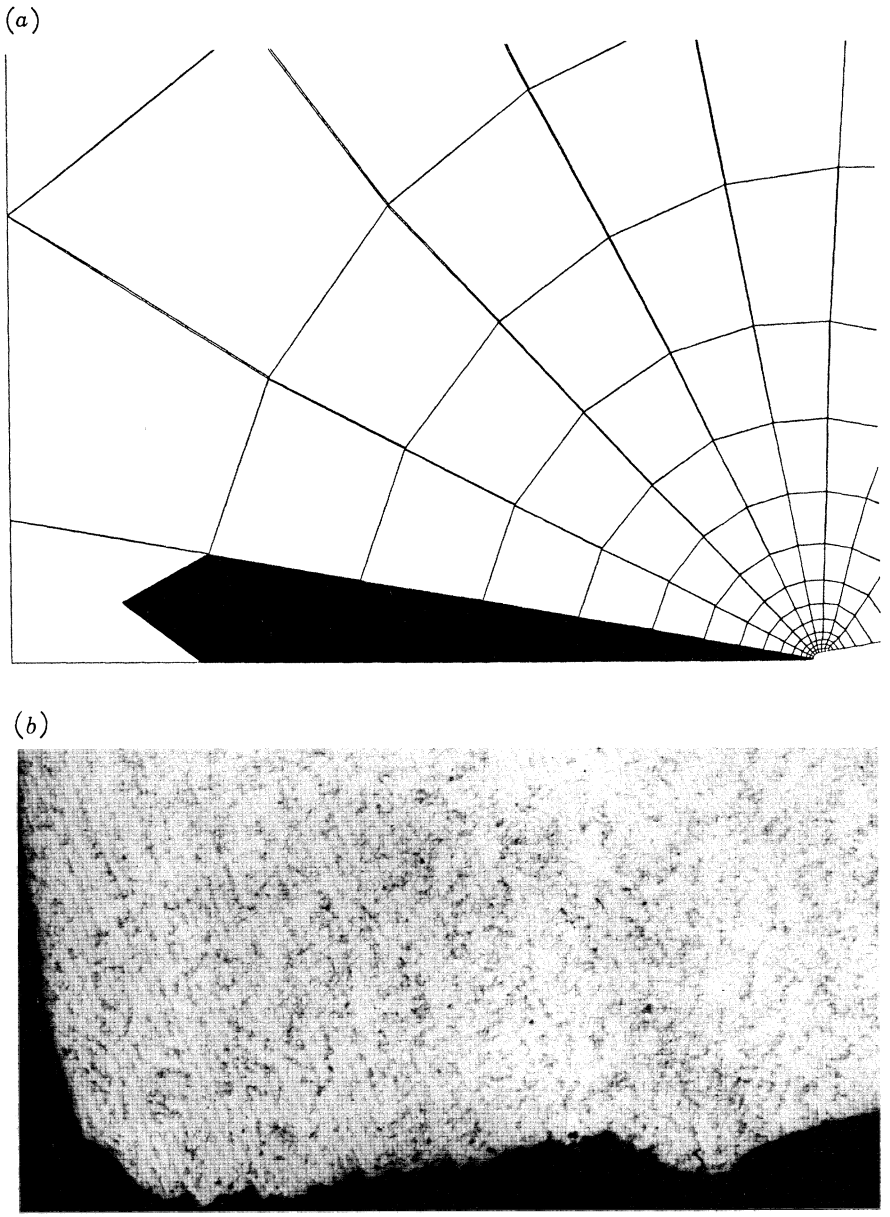

FIGURE 17. Comparison of (*a*) computed failure path, $\omega \geqslant 0.999$, with (*b*) mid-thickness micrograph taken from the minimum section of an internally cracked specimen in 316 stainless steel at failure.

PHILOSOPHICAL TRANSACTIONS OF THE ROYAL SOCIETY A MATHEMATICAL, PHYSICAL & ENGINEERING SCIENCES

an expression for the rupture lifetime t_f may be obtained. At the stress $\hat{\sigma}$ both equations have the same lifetime; this fact may be used to relate C_A, C, χ_A, χ and $\hat{\sigma}$. The two equations which result may be normalized to give

$$\dot{\omega} = \Sigma_A^{\chi}/V_u(1+\phi)\,(1-\omega)^{\phi} \quad \text{for} \quad \Sigma_A \leqslant \hat{\Sigma}_A, \tag{6a}$$

$$\dot{\omega} = \hat{\Sigma}_A^{(\chi-\chi_A)}\,\Sigma_A^{\chi_A}/V_u(1+\phi)\,(1-\omega)^{\phi} \quad \text{for} \quad \Sigma_A > \hat{\Sigma}_A, \tag{6b}$$

where $$\Sigma_A = \alpha\Sigma_{\mathrm{I}} + (1-\alpha)\,\Sigma_{\mathrm{e}}.$$

In the solution of the boundary value problem for the aluminium alloy and copper the applied stress σ_0 need not be specified since V_u is not strongly dependent on σ_0 and, in turn, the value of Σ_{r} is weakly dependent upon V_u. In the case of 316 stainless steel it is necessary to specify σ_0 to determine if the normalized stress Σ_A is above or below $\hat{\Sigma}_A$.

Equations (3), (5) and (6) have been used to solve the boundary value problems defined in figure 1 for the three materials using the data summarized in table 3. The elastic properties used in the solution were defined by using classical relations for an isotropic continuum and the values of E and ν defined in table 3.

(*c*) *Assumptions*

In the numerical method used to solve the boundary value problems it is assumed that during the growth of creep damage the continuum remains elastically isotropic and that Young's modulus and Poisson's ratio remain constant at their initial values. It is known that the generalized elasticity tensor changes as a result of plasticity and creep damage: see, for example, the work of Vavakin & Salganik (1975) and of Chaboche (1979). The influence of such changes on structural behaviour has been assessed by Hayhurst (1976) for beam structures subjected to cyclic loading. Pronounced changes in elastic moduli do not take place until late in life and the overall structural performance is not dramatically affected. This conclusion has been checked by Hayhurst *et al.* (1975*a*) who performed similar calculations on plates and obtained close agreement between experimental and theoretical results.

Probably the principal assumption made is that the numerical model is capable of representing two physical features: first, the growth of widespread continuum damage as in the work of Hayhurst (1973), and second, the growth of sharp cracks as in the work of Hayhurst *et al.* (1984) The latter feature may be carried out provided that the finite element model of the structure is such that the initial elastic singular fields are well represented (Hayhurst & Brown 1984) and that the mesh is judiciously refined in the region of probable crack growth. Experience has shown that it is important to model accurately the region in which early crack growth takes place but, thereafter a coarser model can be tolerated for the region in which subsequent growth takes place.

The assumption of zero dilatation rate, implicit in (2) and (4), is not strictly true, but experimental data, for example those due to Boettner & Robertson (1961), shows that the dilatation is small, under 1 %, until the latter stages of the lifetime when the dilatation can be large. The assumption of zero dilatation has been made by Hayhurst *et al.* (1975*a*) and by Hayhurst *et al.* (1984) in similar structural calculations and they have obtained results which are in close agreement with experimental observations. This is not surprising since Brown *et al.* (1980) have studied axi-symmetrically notched bars in a plastically dilating medium and have concluded that similar estimates of dilatation behaviour may be obtained by using the void growth equations coupled with the results of a notch-analysis for an incompressible plastic material.

PHILOSOPHICAL TRANSACTIONS OF THE ROYAL SOCIETY A MATHEMATICAL, PHYSICAL & ENGINEERING SCIENCES

Also Hutchinson (1983) has studied the effect of dilatation rate on crack-tip fields and has shown that while the stress and strain-rate fields are relatively insensitive to dilatation, they change slightly so that the energy dissipation rates are about the same for a given J. These solutions are valid for near-tip regions and one would expect that for the more realistic situations, where dilatation and dilatation rate fields exist at the crack tip and in which the lifetimes are determined by stress level and stress state, the influence of material dilatation on the overall component lifetime may be small. The assumption of zero dilatation is made in this paper.

The finite element analysis has been formulated for small strains and hence the behaviour of components has been studied at low stress levels where the strains to failure are small; similar situations would be expected under design conditions for in-service components. The method of analysis does not take account of the final mode of failure which inevitably involves the time-independent collapse of a degenerate material; this is not thought to be a serious omission since the process takes place during the final moments of the lifetime.

(*d*) *Numerical models*

In the work to be described later it was found necessary to model two types of cracked members: first, the laboratory geometry specified earlier, and second, their line-crack equivalents. The crack tip mesh geometry used for the latter situation has been discussed by Hayhurst & Brown (1984). In plane strain situations, well known numerical difficulties are encountered when the finite element displacement method is used to achieve pointwise incompressibility in stationary-state problems. The growth of the damage variable ω ensures the presence of a degree of elasticity and this difficulty is not so severe. However, Nagtegaal *et al.* (1974) have shown that a few conventional element-types can be used, including the 3-node constant strain element, in special arrangements to achieve pointwise incompressibility. Such an arrangement has been used here; the triangular elements are formed by joining the diagonals of a general quadrilateral, the exact point of intersection forming the common node of four elements. The plane strain computations were done for a single quadrant of the specimen ($b \geqslant x \geqslant 0$, $h \geqslant y \geqslant 0$) shown in figure 1. The finite element models had $h/b = 3$, 568 and 640 constant strain triangles, 309 and 351 nodes, for the line-crack and laboratory geometries respectively. The boundary defined by $y = +h$ was subjected to the constant stress $\Sigma_{yy} = 1$. Values of the uniform applied stress σ_0 need not be specified for the aluminium alloy and the copper materials due to the form of the normalization adopted. But in the case of the stainless steel it is necessary to specify σ_0 due to the bilinear rupture curve (figure 5). The values of σ_0 used were taken from the low ends of the experimental data presented by Hayhurst *et al.* (1981). The computations were done in double precision on the Science and Engineering Research Council IBM 360/195 computer at the Rutherford and Appleton Laboratory, Chilton. Computer times ranged from 24 min for the internally cracked stainless steel specimen, to 47 min for the externally cracked copper specimen. Numerical results are presented in the next section.

5. Results

The values of Σ_r computed for the laboratory specimen geometries, shown in figure 1, are compared with the corresponding experimental values, corrected for changes in specimen geometry, in table 4. Close agreement may be observed in all cases between the results of experiment and theory; the agreement is least good for the internally cracked 316 stainless steel specimen

for which the theoretical value of Σ_r is 4 % higher than the corresponding experimental value; this difference is not significant relative to the scatter found in uni-axial creep rupture data.

More detailed experimental and theoretical results are presented for all specimens and materials in the following subsections. All of the micrographs presented have been taken from mid-thickness planes in the region of the minimum section of each specimen; the regions shown in the micrographs extend from the centre-line of the externally cracked specimens to the crack-tip region, and from the edges of the internally cracked specimens to the crack-tip region, unless otherwise stated. Also presented for both specimen types, in the aluminium alloy and in copper, are theoretical predictions of failure paths, defined by $\omega \geqslant 0.999$, or crack advancement over the same regions. In addition, contour plots of theoretical predictions of creep damage and stress states are given over regions which encompass one half of the minimum section of the specimens.

TABLE 4. COMPARISON OF CORRECTED EXPERIMENTAL WITH THEORETICAL VALUES OF THE NORMALIZED REPRESENTATIVE RUPTURE STRESS OBTAINED FOR THE LABORATORY SPECIMEN GEOMETRY

		normalized representative rupture stress Σ_r	
		internal	external
material	case	crack	crack
aluminium alloy	experiment	1.00	0.78
	theory	0.99	0.78
copper	experiment	1.01	0.87
	theory	1.02	0.88
316 stainless steel	experiment	1.25	0.93
	theory	1.30	0.91

(*a*) *Aluminium alloy*

The internally and externally cracked aluminium specimens were first modelled theoretically with the geometry for the laboratory specimens, given in figure 1. Although the theoretical predictions for Σ_r for this model were in close agreement with the experimentally derived values, table 4, the predictions of the regions of intense damage, $\omega \geqslant 0.999$, were not compatible with the experimentally observed damage distributions shown in figure 3 for the aluminium alloy (D19S), and in figures 6*b*, plate 2, and 7*b*, plate 3, for the aluminium alloy being studied here. In all three situations extensive damage may be observed on planes inclined at approximately 55° to the x-axis. The theoretical predictions showed that a narrow region of failed material spread out from the crack-tip along the plane of the minimum section, while the levels of damage were relatively low on planes inclined at approximately 55° to the x-axis, for the internally and externally cracked specimens. Examination of unfailed test specimens showed that a short crack grew on load up, in the plane of the initial crack, which has the effect of sharpening the initial machined crack. For this reason the laboratory geometries were idealized as line-cracks. The values of the representative rupture stress Σ_r, computed for the externally and internally line-crack equivalent specimens, are 0.74 and 1.01 respectively. The external and internal line-crack equivalents show more strengthening and weakening, respectively, than the corresponding results for the laboratory specimens, but the differences between the two sets of values are small. The regions of failed material predicted for the line-crack equivalent specimens are given in figures 6*a*, plate 2, and 7*a*, plate 3, for the external crack close to failure and for the internal crack at 95 % of life respectively. They both show that cracks have developed on planes inclined at approximately 55° to the x-axis. In the case of the externally cracked specimen it is also

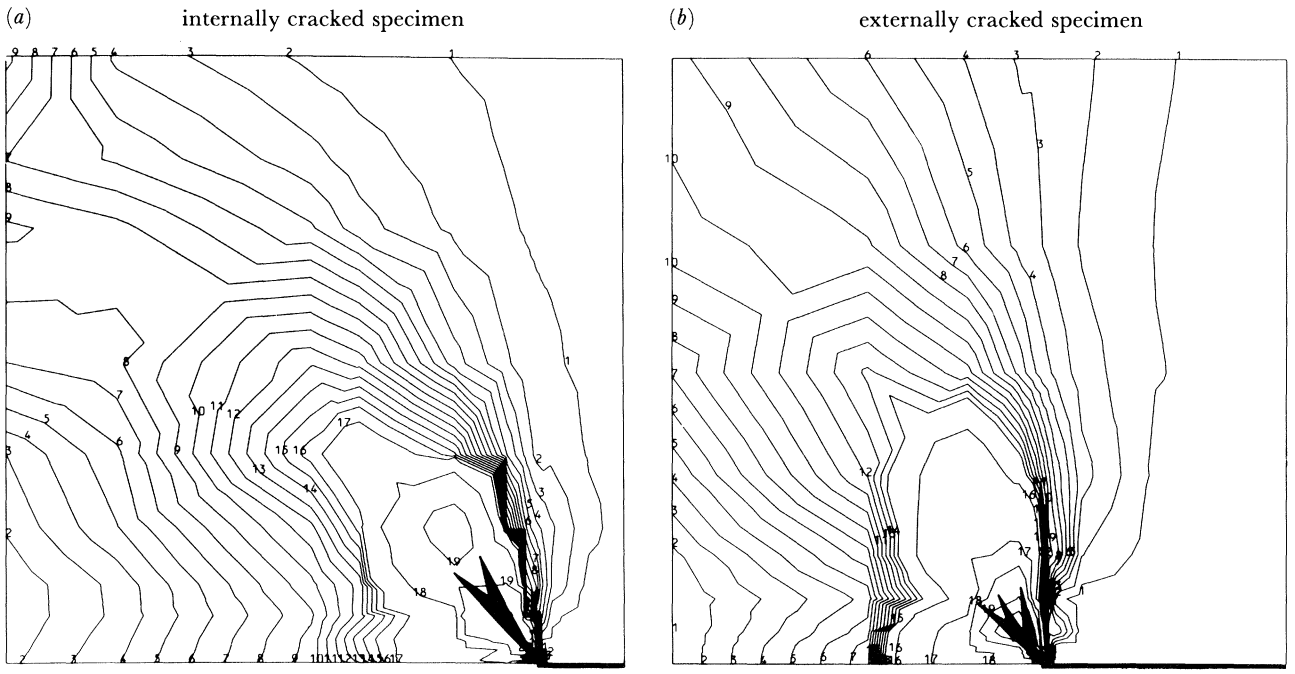

FIGURE 8. For description see opposite.

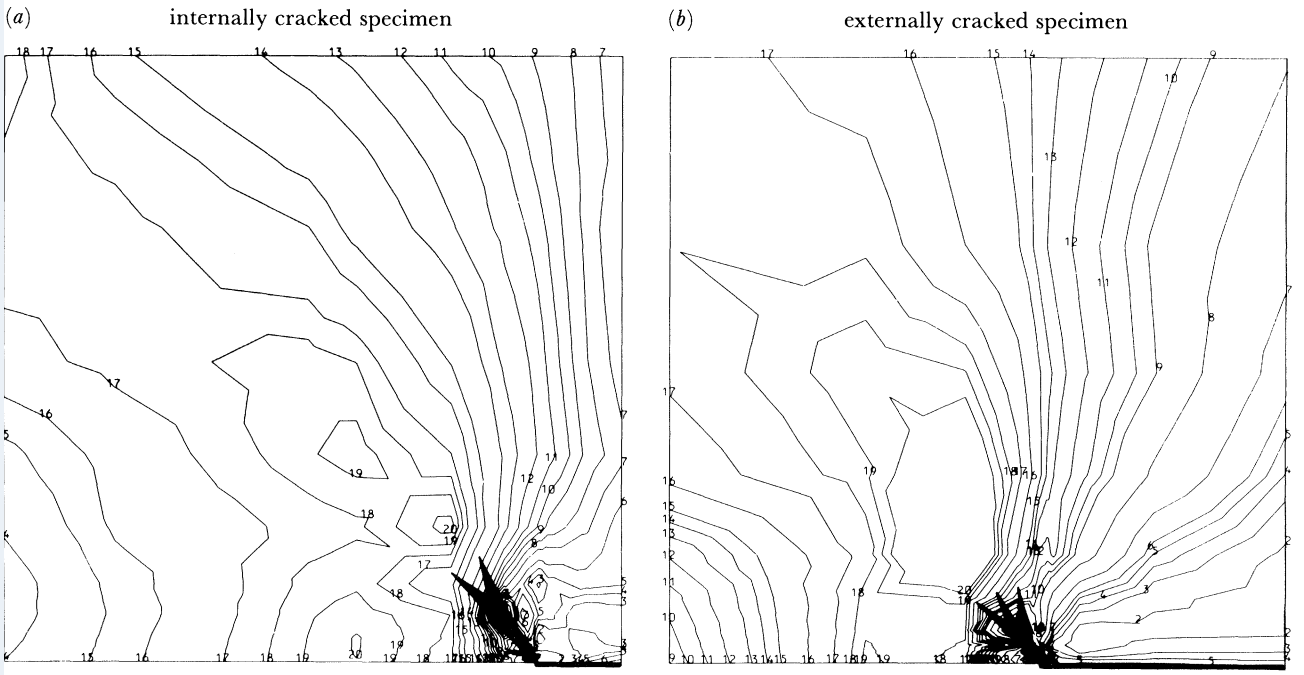

FIGURE 9. For description see opposite.

predicted (figure 6*a*) that a crack propagates from the centre-line of the specimen, along the x-axis, towards the crack tip; this event is predicted to take place very close to failure and models the final collapse mechanism. The computed states of crack advance (figures 6*a* and 7*a*) may be compared with mid-thickness micrographs (figures 6*b* and 7*b*) taken from specimens at the corresponding life fractions. In both cases grain boundary damage, in the form of short fissures, may be observed to have grown on the predicted shear planes. In the case of the externally cracked specimen separation takes place by the advancement of a crack along the plane of the minimum section, as predicted in figure 6*a* whereas, in the case of the internally cracked member failure takes place by a 'slide-off' mechanism along the predicted shear plane (figure 7*a*). It is of interest to contrast this mechanism with that for the externally cracked specimen in the D19S material shown in figure 3, where the material separates on the shear plane, inclined at 55° to the x-axis, and on a plane that connects the tips of the shear planes, on opposite sides of the specimen, immediately before failure.

In figures 8*a* and *b* computed contours of constant damage are given for the internally and externally cracked specimens at 60 % of life for the aluminium alloy; also shown in the figures is the manner in which the initial cracks have propagated. Damage values ahead of the propagated cracks are of the order $\omega = 0.15$. The damage distribution between the propagated crack and the x-axis is more intense in the case of the externally cracked specimen. This situation is more pronounced before collapse when the centre of the specimen, close to the x-axis, is subjected to

FIGURE 8. Comparison of minimum cross section plots of creep damage for internally and externally cracked specimens at $t/t_t = 0.6$ in an aluminium alloy.

(*a*) Base of square region defined by $b \geqslant x \geqslant \frac{2}{9}b$. Contour numbers 1–20 correspond to heights of

1: 0.002;	2: 0.005;	3: 0.008;	4: 0.011;
5: 0.014;	6: 0.017;	7: 0.020;	8: 0.022;
9: 0.026;	10: 0.029;	11: 0.032;	12: 0.035;
13: 0.038;	14: 0.041;	15: 0.044;	16: 0.047;
17: 0.052;	18: 0.084;	19: 0.155;	20: 0.689.

(*b*) Base of square region defined by $\frac{5}{9}b \geqslant x \geqslant 0$. Contour numbers 1–20 correspond to heights of

1: 0.002;	2: 0.005;	3: 0.008;	4: 0.012;
5: 0.015;	6: 0.018;	7: 0.021;	8: 0.025;
9: 0.028;	10: 0.031;	11: 0.035;	12: 0.038;
13: 0.041;	14: 0.044;	15: 0.048;	16: 0.063;
17: 0.114;	18: 0.182;	19: 0.346;	20: 0.599.

FIGURE 9. Comparison of minimum cross section plots of the normalized effective stress σ_e/σ_0 for internally and externally cracked specimens at $t/t_t = 0.6$ in an aluminium alloy.

(*a*) Base of square region defined by $b \geqslant x \geqslant \frac{2}{9}b$. Contour numbers 1–20 correspond to heights of

1: 0.204;	2: 0.385;	3: 0.463;	4: 0.506;
5: 0.540;	6: 0.585;	7: 0.645;	8: 0.690;
9: 0.732;	10: 0.770;	11: 0.812;	12: 0.874;
13: 0.966;	14: 1.057;	15: 1.213;	16: 1.299;
17: 1.408;	18: 1.467;	19: 1.516;	20: 1.571.

(*b*) Base of square region defined by $\frac{5}{9}b \geqslant x \geqslant 0$. Contour numbers 1–20 correspond to heights of

1: 0.124;	2: 0.217;	3: 0.348;	4: 0.434;
5: 0.508;	6: 0.583;	7: 0.760;	8: 1.028;
9: 1.238;	10: 1.312;	11: 1.395;	12: 1.488;
13: 1.581;	14: 1.647;	15: 1.704;	16: 1.819;
17: 1.923;	18: 1.994;	19: 2.041;	20: 2.087.

PHILOSOPHICAL TRANSACTIONS OF THE ROYAL SOCIETY A MATHEMATICAL, PHYSICAL & ENGINEERING SCIENCES

high values of the normalized effective stress σ_e/σ_0. These observations are consistent with the propagation of a single crack from the centre of the specimen at failure since for this material $\alpha = 0$. It is evident from figure 8 that for both specimens cracks advance through relatively lowly damaged material.

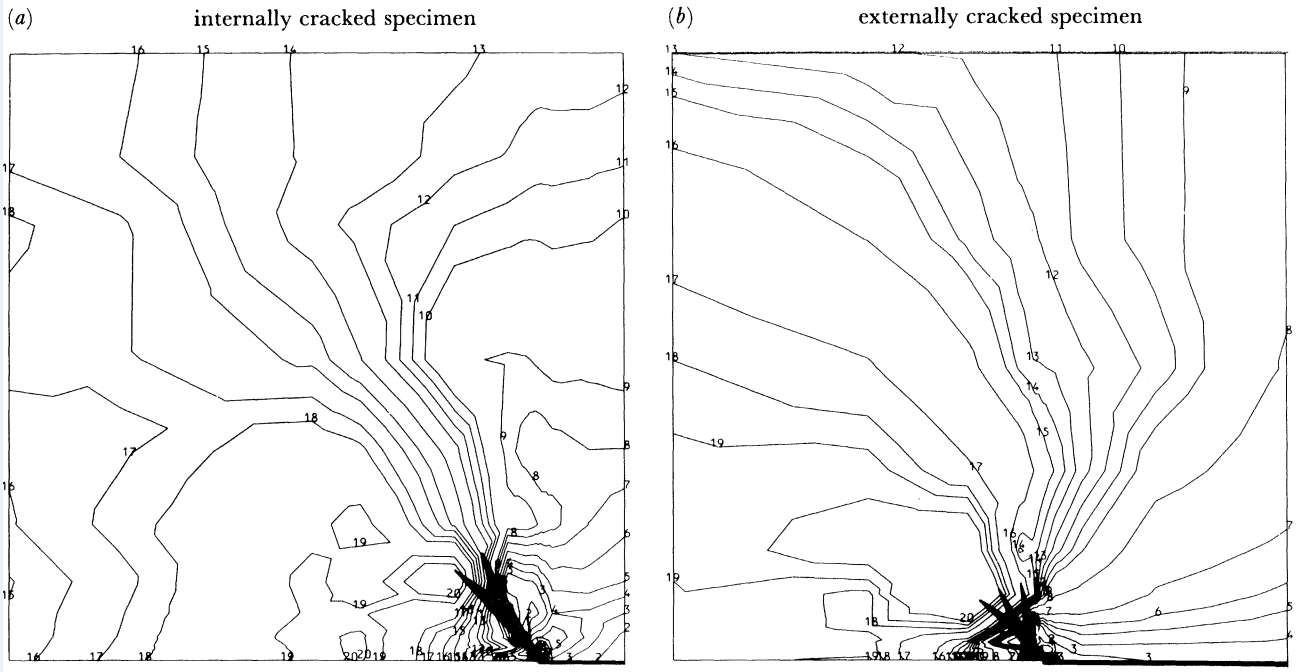

FIGURE 10. Comparison of minimum cross section plots of the normalized first stress invariant J_1/σ_0 for internally and externally cracked specimens at $t/t_f = 0.6$ in an aluminium alloy.

(a) Base of square region defined by $b \geqslant x \geqslant \frac{2}{9}b$. Contour numbers 1–20 correspond to heights of

1: −0.992;	2: −0.735;	3: −0.517;	4: −0.387;
5: −0.267;	6: −0.125;	7: 0.035;	8: 0.165;
9: 0.285;	10: 0.647;	11: 0.788;	12: 0.930;
13: 1.090;	14: 1.358;	15: 1.637;	16: 1.849;
17: 2.125;	18: 2.343;	19: 2.988;	20: 3.300.

(b) Base of square region defined by $\frac{5}{9}b \geqslant x \geqslant 0$

1: −1.765;	2: −0.904;	3: −0.626;	4: −0.392;
5: −0.197;	6: −0.022;	7: 0.320;	8: 1.012;
9: 1.481;	10: 1.666;	11: 1.852;	12: 2.037;
13: 2.230;	14: 2.424;	15: 2.619;	16: 3.082;
17: 4.277;	18: 4.969;	19: 5.384;	20: 5.940.

In figure 9 contours of constant normalized effective stress, σ_e/σ_0, are given for both specimens at the same stage in the lifetime as in figure 8. For both specimens the value of σ_e/σ_0 is highest in the region ahead of the propagated crack, but similar values are found close to the x-axis. The regions of high σ_e/σ_0, ahead of the propagated crack, extend over a large region in a direction inclined at an approximate angle of 50–55° to the x-axis. Since the aluminium alloy ruptures according to a maximum σ_e/σ_0 criterion, or $\alpha = 0$, it is not surprising that the zones of high damage shown in figure 8 coincide with the zones of high σ_e/σ_0.

In figure 10 contours of constant normalized first stress invariant J_1/σ_0 are given for both specimens at the same stage in the lifetime as in figures 8 and 9. The distributions are similar to

those for the maximum principal tension stress, and contours for the latter are not presented here. For both specimens the regions of high J_1/σ_0 occur below and touching the plane that contains the propagating crack; the values of the normalized effective stress σ_e/σ_0 tend to be low in the same regions. A similar characteristic was observed in the case of a British Standard v-notched specimen made from 316 stainless steel for which the crack propagation plane was inclined at a small angle to the plane of the original notch (Hayhurst *et al.* 1984).

Examination of the magnitudes of the stresses in figures 9 and 10 suggests that the effect of the growth of damage has been to redistribute stress; this aspect of the results is discussed further in a later section.

(*b*) *Copper*

The internally and externally cracked copper specimens were modelled with the geometry for the laboratory specimens, given in figure 1. Unlike the aluminium alloy specimens no experimental evidence was found of the propagation of sharp cracks on load up, hence one is justified in using the initial specimen geometry. The influence of subsequent finite deformations will be discussed in a later section. Theoretical predictions of the crack advancement are shown in figure 11*a*, plate 4, for the externally cracked specimen at 94 % of life, and in figure 12*a*, plate 5, for the internally cracked specimen at 99 % of life; the predictions are compared with the distributions of grain boundary damage shown in the micrographs, taken from mid-thickness planes, presented in figures 11*b*, plate 4, and 12*b*, plate 5. For both specimens the grain boundary damage can be observed to have formed and linked up producing cracked regions that are similar in shape and orientation to those predicted theoretically. It is predicted theoretically that both specimens separate on planes that contain the propagated cracks shown in figures 11*a* and 12*a*. These predictions are not accurate since the experimental results show that the specimens separate on the minimum section planes. The predictions are not seriously in error since the material in the regions between the plane of the minimum section and the theoretical plane of crack propagation, are intensively damaged (cf. figures 11*b* and 12*b*) and in addition the event takes place at the end of the lifetime.

In figures 13*a* and *b* computed contours of constant damage are given for the internally and externally cracked specimens at 60 % of life; also shown is the manner in which the initial cracks have propagated. In both cases higher levels of damage, of the order of $\omega = 0.28$, can be seen to have formed on the planes of the propagating cracks that extend either to the edge of the specimen, for the internally cracked specimen, or to the centre-line, in the case of the externally cracked specimen. The distributions for the externally cracked specimen are different since the region between the plane of the propagating crack and the plane of the minimum section is reasonably uniformly damaged. Comparison of the damage distributions shown in these figures with those presented for the aluminium alloy specimens (figure 8) shows that the copper specimens undergo more widespread damage.

In figure 14 contours of constant normalized effective stress, σ_e/σ_0, are given for both specimens at the same stage in the lifetime as given in figure 13. For both specimens the regions of highest σ_e/σ_0 occur immediately below the tip of the propagated crack and extend outwards towards the x-axis. The same feature was observed in numerical solutions for creep crack advancement in an axi-symmetrically v-notched tension bar in 316 stainless steel studied by Hayhurst *et al.* (1984).

In figure 15 contours of constant normalized first stress invariant J_1/σ_0 are given for both specimens at the same stage in life as that given in figures 13 and 14. The distributions are

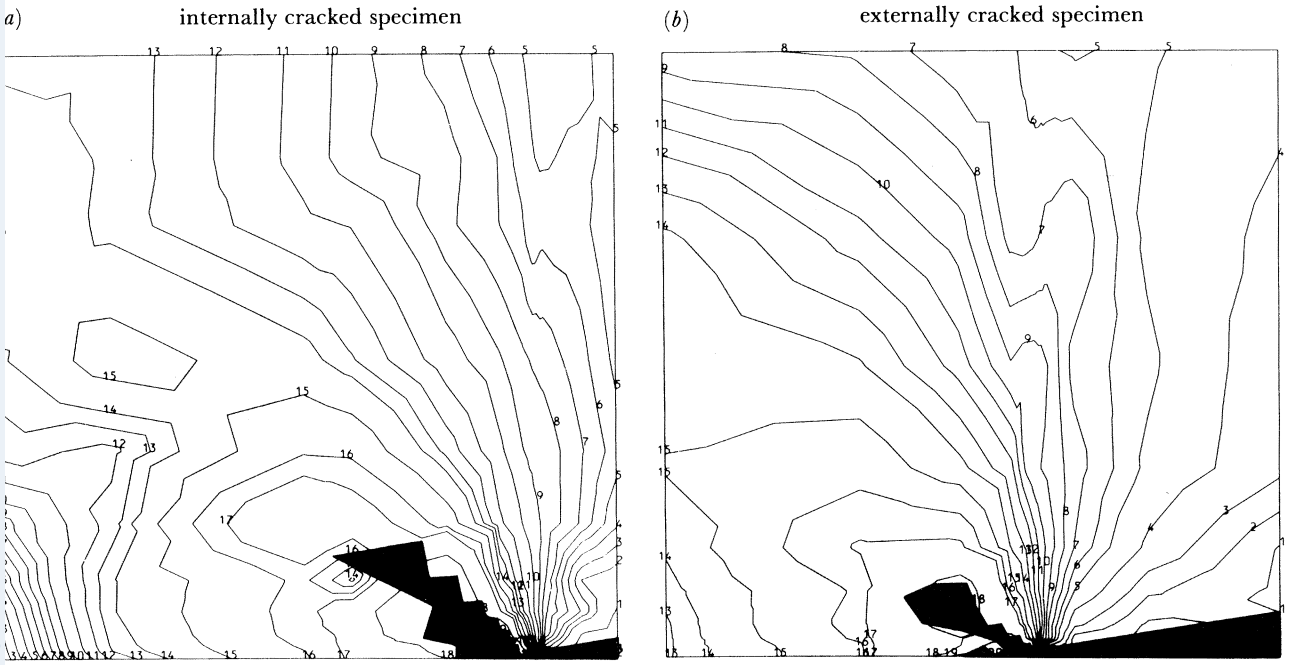

FIGURE 13. For description see opposite.

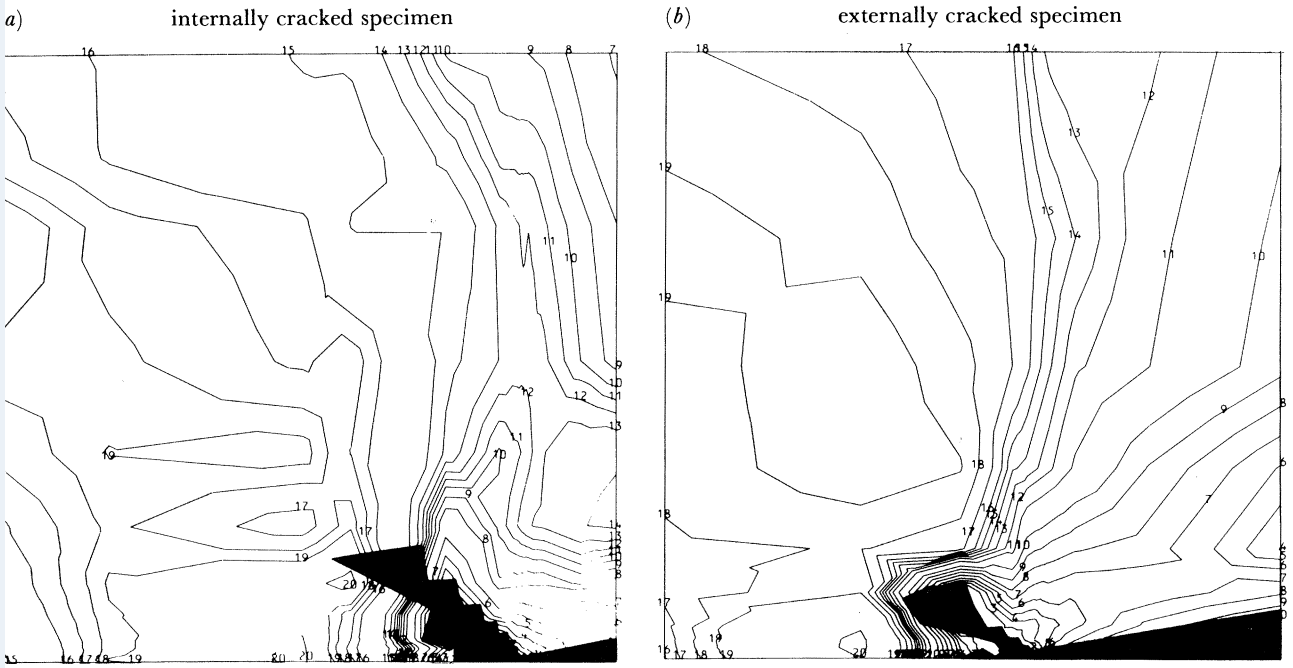

FIGURE 14. For description see opposite.

PHILOSOPHICAL TRANSACTIONS OF THE ROYAL SOCIETY A MATHEMATICAL, PHYSICAL & ENGINEERING SCIENCES

similar to those for the maximum principal tension stress and contours for the latter are not presented here. In the case of the internally cracked specimen, the region of highest J_1/σ_0 occurs ahead of the propagated crack and extends towards the x-axis. This region coincides with the region of highest damage (figure 13); hence the crack propagates into the region since the rupture of copper is principally controlled by the maximum principal tension stress or $\alpha = 0.7$. In the case of the externally cracked specimen the region of highest J_1/σ_0 occurs at the point ($x = 0$, $y = 0$); the region between this point and the tip of the propagating crack is subjected to a relatively high value of J_1/σ_0. However, a region of failed material does not develop here since the region does not coincide with the zone of most intensely damaged material. Instead the crack propagates into the region of high damage where J_1/σ_0 is moderately high.

In both copper specimens crack advancement does not take place on the plane of the minimum section since the rupture criterion is a mixed one and is influenced by the magnitude of σ_e/σ_0. It is this characteristic that results in crack advancement along a plane inclined at an angle of approximately 30–40° to the x-axis.

(*c*) 316 *stainless steel*

The internally and externally cracked stainless steel specimens were modelled with the geometry for the laboratory specimens, given in figure 1. No experimental evidence of the propagation of sharp cracks was obtained on initial loading. Initial geometry changes were

---

FIGURE 13. Comparison of minimum cross section plots of creep damage for internally and externally cracked specimens at $t/t_f = 0.6$ in copper.

(*a*) Base of square region defined by $b \geqslant x \geqslant \frac{2}{9}b$. Contour numbers 1–20 correspond to heights of

1: 0.029;	2: 0.062;	3: 0.076;	4: 0.091;
5: 0.105;	6: 0.118;	7: 0.129;	8: 0.140;
9: 0.152;	10: 0.165;	11: 0.186;	12: 0.207;
13: 0.226;	14: 0.245;	15: 0.284;	16: 0.335;
17: 0.386;	18: 0.598;	19: 0.917;	20: 0.983.

(*b*) Base of square region defined by $\frac{5}{9}b \geqslant x \geqslant 0$. Contour numbers 1–20 correspond to heights of

1: 0.016;	2: 0.036;	3: 0.056;	4: 0.081;
5: 0.106;	6: 0.120;	7: 0.135;	8: 0.149;
9: 0.163;	10: 0.178;	11: 0.192;	12: 0.207;
13: 0.225;	14: 0.244;	15: 0.282;	16: 0.335;
17: 0.386;	18: 0.762;	19: 0.874;	20: 0.979.

FIGURE 14. Comparison of minimum cross section plots of the normalized effective stress σ_e/σ_0 for internally and externally cracked specimens at $t/t_f = 0.6$ in copper.

(*a*) Base of square region defined by $b \geqslant x \geqslant \frac{2}{9}b$. Contour numbers 1–20 correspond to heights of

1: 0.027;	2: 0.081;	3: 0.183;	4: 0.282;
5: 0.359;	6: 0.430;	7: 0.530;	8: 0.673;
9: 0.727;	10: 0.774;	11: 0.809;	12: 0.845;
13: 0.889;	14: 0.955;	15: 1.063;	16: 1.483;
17: 1.621;	18: 1.747;	19: 1.839;	20: 2.096.

(*b*) Base of square region defined by $\frac{5}{9}b \geqslant x \geqslant 0$. Contour numbers 1–20 correspond to heights of

1: 0.045;	2: 0.136;	3: 0.380;	4: 0.480;
5: 0.571;	6: 0.663;	7: 0.788;	8: 0.912;
9: 1.036;	10: 1.170;	11: 1.375;	12: 1.501;
13: 1.584;	14: 1.660;	15: 1.719;	16: 1.777;
17: 1.875;	18: 2.017;	19: 2.188;	20: 3.122.

PHILOSOPHICAL TRANSACTIONS OF THE ROYAL SOCIETY A MATHEMATICAL, PHYSICAL & ENGINEERING SCIENCES

observed but these will be shown in a later section not to be significant. Theoretical predictions of crack advancement are shown in figure 16*a*, plate 6, for the externally cracked specimen at 60 % of life, and in figure 17*a*, plate 7, for the internally cracked specimen almost at failure; the predictions are compared with the distributions of grain boundary damage shown in the micrographs in figures 16*b*, plate 6, and 17*b*, plate 7. For both specimens the grain boundary damage can be observed to have formed and linked up producing cracked regions that are similar in shape and orientation to those obtained theoretically.

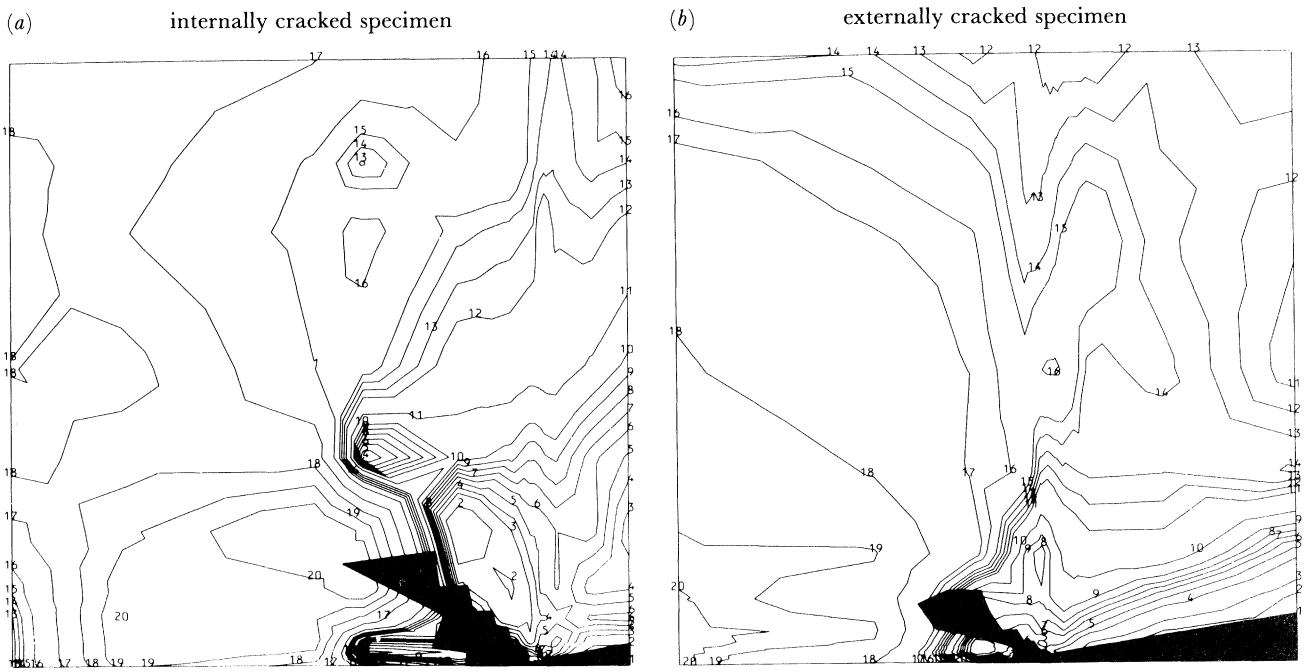

FIGURE 15. Comparison of minimum cross section plots of the normalized first stress invariant J_1/σ_0 for internally and externally cracked specimens at $t/t_f = 0.6$ in copper.

(*a*) Base of square region defined by $b \geqslant x \geqslant \frac{2}{9}b$. Contour numbers 1–20 correspond to heights of

1: −1.501;	2: −0.862;	3: −0.576;	4: −0.456;
5: −0.336;	6: −0.221;	7: −0.131;	8: −0.040;
9: 0.050;	10: 0.140;	11: 0.323;	12: 0.620;
13: 0.759;	14: 0.898;	15: 1.036;	16: 1.385;
17: 2.157;	18: 2.938;	19: 3.633;	20: 4.301.

(*b*) Base of square region defined by $\frac{5}{9}b \geqslant x \geqslant 0$. Contour numbers 1–20 correspond to heights of

1: −1.914;	2: −1.662;	3: −1.326;	4: −0.769;
5: −0.475;	6: −0.222;	7: −0.036;	8: 0.150;
9: 0.400;	10: 0.836;	11: 1.517;	12: 1.752;
13: 1.987;	14: 2.268;	15: 2.562;	16: 3.271;
17: 3.775;	18: 6.395;	19: 8.993;	20: 9.424.

In both cases initial crack advance takes place along the plane of the minimum section because of creep. It does so relatively rapidly since the stresses are typically greater than the stress $\hat{\sigma}$ defined in figure 5. After the crack has advanced a short distance in this manner, the rate of propagation reduces after stress redistribution has lowered the typical stress levels below $\hat{\sigma}$. After this event the two specimens behave differently. The theoretical predictions for the externally cracked specimen, with $\sigma_n = 241.33$ MPa, show that the plane of crack advancement deviates

from the plane of the minimum section to one which is almost parallel to the y-axis. Final failure takes place by the region between the current crack front and the y-axis behaving as a relatively uniformly stressed region; the entire section fails at the same instant in the manner described, by Hayhurst *et al.* (1981). This result is typical of theoretical predictions obtained for lower and slightly higher levels of applied stress. In the case of the internally cracked specimens failure is predicted to take place in the plane of the minimum section and this result is corroborated by the mid-thickness micrograph given in figure 17*b*. However, these results were obtained for a value of $\sigma_n = 210.30$ MPa and experimental results for higher stresses showed that the plane of the propagating crack deviates slightly from the plane of the minimum section, as described by Hayhurst *et al.* (1981). The theoretical values of Σ_r, at slightly higher stresses, were not significantly affected. Theoretical contour plots of damage and stress states have not been presented here for stainless steel since they are similar to those for copper. This is to be expected since the value of α for the multi-axial stress rupture criteria is 0.75 which is close to the value of 0.70 for copper.

6. Discussion

The theoretical results for the internally and externally cracked aluminium alloy specimens clearly show that if the crack is not to propagate in the plane of the minimum section then the conditions at the tip of the sharp crack, produced on initial loading, must be accurately modelled. When this is done it is predicted that the crack propagates in a plane inclined at an angle of approximately 50–55° to the plane of the minimum section. In the case of the theoretical result for copper, crack propagation does not take place in the plane of the minimum section when the laboratory specimen geometry is assumed; this result is not consistent with the result for the aluminium alloy. A possible explanation could stem from the fact that the aluminium alloy has a low rupture ductility, approximately 1 %, and the copper has a rupture ductility in the region of 4–8 %. It is significant that none of the failure modes determined here would have been predicted by the methods discussed in § 3.

In the case of copper, and to a much greater extent for 316 stainless steel, finite plastic straining was encountered on initial loading. For 316 stainless steel the change in the crack-tip geometry was measured experimentally and modelled by using the finite element method. The predictions of the representative rupture stress Σ_r and of the manner in which the crack propagates were essentially unaltered despite significant changes of the crack opening and of the radius of the crack-tip. The inference of this result is that the detail of the crack-tip geometry is not too important and good predictions of lifetime may be obtained if the changes in net-section stress are taken into account. Similar conclusions have been drawn by Ohtani (1981).

The importance of the inclusion of elastic effects is not easy to judge for the cases studied here without repeating the computations with the elastic terms omitted; this is an onerous task which has not been attempted.

The following assumptions were made:

(i) that Young's modulus and Poisson's ratio remain constant and independent of damage;

(ii) that creep rupture takes place with zero dilatation.

The good agreement obtained between theoretical and experimental results suggests these assumptions are accurate.

The effects of stress redistribution upon the shape of the spatial stress distributions across the plane of the minimum section are now discussed for the externally cracked copper specimen.

PHILOSOPHICAL TRANSACTIONS OF THE ROYAL SOCIETY A MATHEMATICAL, PHYSICAL & ENGINEERING SCIENCES

This particular case has been selected since it is characteristic of all the other cases studied. The spatial distributions of normalized axial stress are given, at different times, in figure 18, for the minimum section in terms of the normalized coordinate $x/(b-a)$. At zero time the singular character of the stress field may be observed; at the centroid of the crack-tip element a normalized stress of 18 occurs. At 0.44 % of life a number of elements have failed at the tip of the original crack, where the mesh is sufficiently fine to model a sharp crack. Despite this, the distribution has lost its singular character owing to the formation of damage and the stress redistribution that results. Further elapse of time results in the failure of more elements and the propagation of the crack along the minimum section. The normalized stress distributions at the normalized times, 4.4×10^{-3}, 2.7×10^{-2} and 8.1×10^{-2} show characteristics similar to those for the continuum

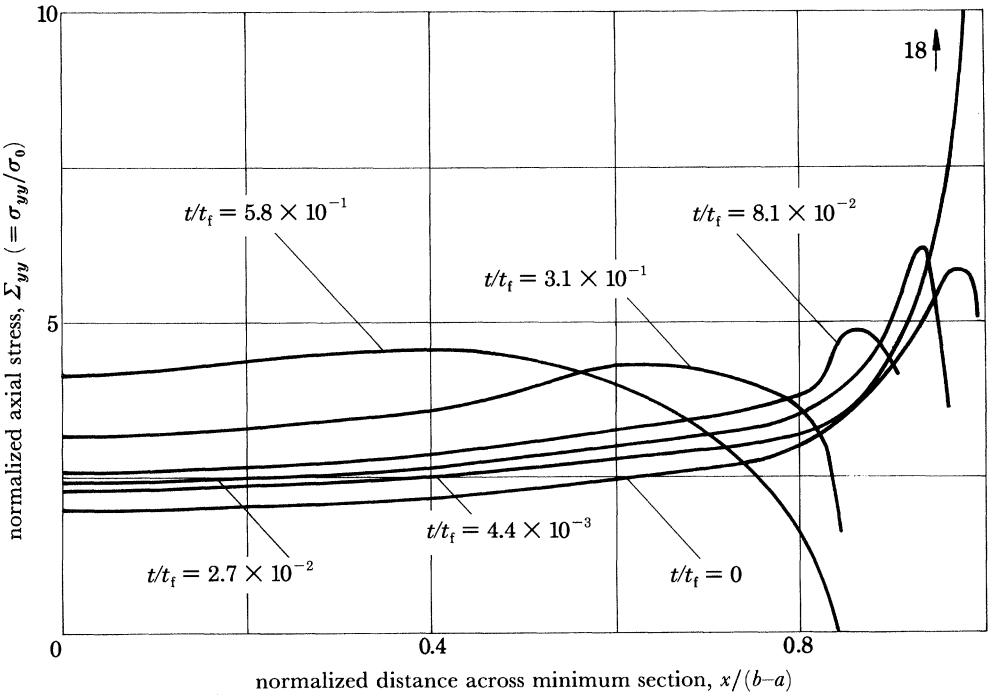

FIGURE 18. Change in the variation of normalized axial stress across the minimum section with normalized time for an externally cracked copper specimen.

damage solutions of British Standard circumferentially v-notched tension bars due to Hayhurst *et al.* (1984). After the normalized time 3.1×10^{-1}, crack propagation takes place mainly away from the minimum section and the formation of widespread damage results in relatively uniform states of stress; this is so even in the plane of the propagating crack (cf. figures 14 and 15). It is of interest to examine the character of the distributions of the strain rates across the plane of the minimum section. The numerical method did not involve the evaluation of total strain rates and instead the spatial variations of the normalized creep strain rates (equal to $\dot{v}_e/e_0$) are given in figure 19. At zero time the singular distribution may be observed; as time elapses the failure of elements takes place and the distributions still preserve an approximate singular character for 2.7 % of the lifetime. Thereafter the distributions are less extreme, and after 31 % of life they develop a relatively smooth character. This behaviour is also reflected in the region of the plane

of the propagating crack. The effect of the growth of continuum damage in the cracked bodies is to weaken, and to nullify eventually, the singular stress and creep strain-rate distributions.

Finite element meshes with different numbers of degrees of freedom were used and it was found that the initial elastic singular fields and the regions through which early crack growth take place should both be modelled accurately. By the time the crack has extended by, say, 10 % of its initial length the influence of damage upon the stress field is to nullify the singularity so that the regions through which subsequent crack growth takes place can be modelled with coarser elements. Although in the figures presented here relatively coarse elements may be observed, the computed values of Σ_r may not be significantly improved by further mesh refinement with constant strain triangles.

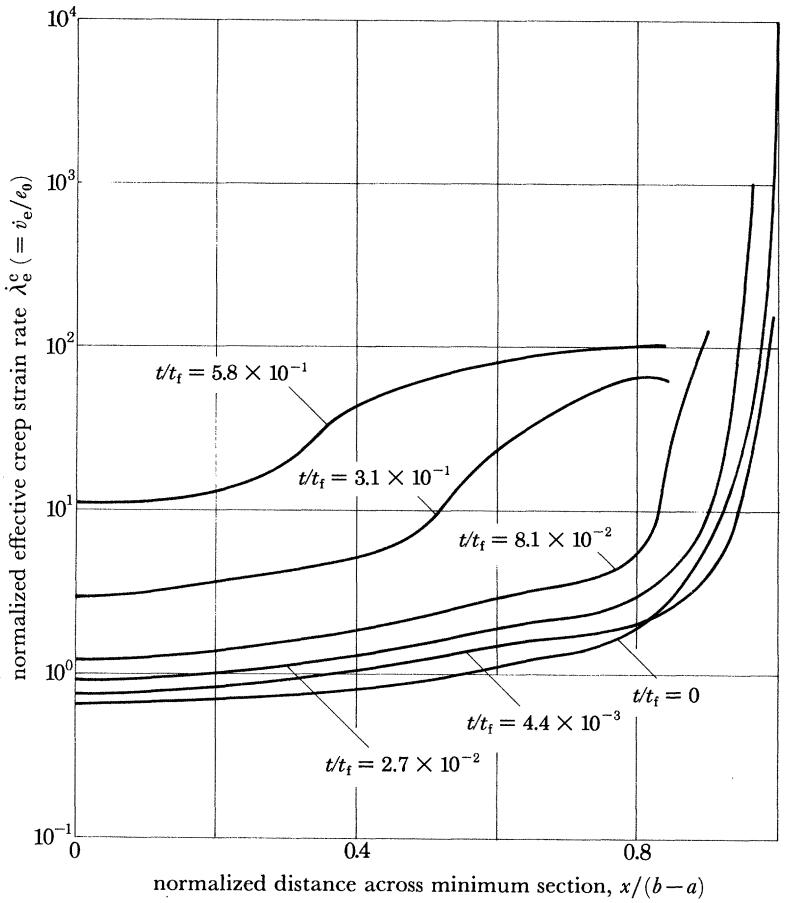

FIGURE 19. Change in the variation of the normalized effective creep strain rate across the minimum section with normalized time for an externally cracked copper specimen.

The numerical method used here has the advantage that once the material behaviour has been correctly modelled by the constitutive equation the precise mechanism of crack growth is automatically determined for a particular cracked body. This feature may have appeal to designers or to those assessing the integrity of cracked components. If the method is to become a viable proposition, then either computer times need to be reduced or faster and more economical computers developed.

7. Conclusions

A finite element computer program previously developed to study the growth of continuum damage in axi-symmetrically notched tension bars has been used to study crack growth in externally and internally cracked, plane strain, tension members under steady load in an aluminium alloy, in copper and in 316 stainless steel. In all cases the predicted lifetimes, expressed in terms of a representative rupture stress, have been shown to be in very close agreement with experimentally determined values. The theoretical method has been used to predict distributions of damage obtained from metallographic examination of mid-thickness sections taken from test specimens.

The theory of continuum damage mechanics has been shown to be capable of predicting the growth of sharp cracks through relatively lightly damaged material. The mechanism by which this takes place involves the interaction between the complex states of stress, found to occur in plane strain cracked bodies, and the multi-axial stress rupture criterion of the material, through the agency of stress redistribution due to continuum damage. The choice of plane upon which crack propagation takes place is dependent on the multi-axial stress rupture criterion of the material, the geometry of the cracked body and the loading conditions.

The principal effect of continuum damage is to weaken the strength of the singular stress fields and eventually to nullify them. In the case of the creep strain rate fields the same effect is encountered, but in a less pronounced way.

Previous studies have assumed that the stresses, at the tip of a propagating crack, are given by the H.R.R. fields and have used them in conjunction with suitable void growth models to study creep crack growth. The results of these investigations must be questioned for the following reasons:

(i) the growth of continuum damage as a field quantity has been omitted and hence the stresses are overestimated at the crack-tip and underestimated elsewhere;

(ii) the multi-axial stress rupture behaviour is usually not accurately modelled and hence the crack is confined to propagate in the plane of the original crack.

The results presented here show that the initial crack geometry is important in the case of the aluminium alloy specimens, but this is not so for the copper and the 316 stainless steel specimens. This is probably because of the particular aluminium alloy having a low rupture ductility. The most important geometry change, also reported by Ohtani (1981), is the reduction in the area of the minimum section.

The numerical method of solution used here has the advantage that it automatically selects the appropriate mechanism of crack growth provided that tertiary creep strains and the multi-axial stress rupture behaviour are modelled by the constitutive equations. This feature may appeal to designers and to those wishing to assess the integrity of cracked components.

The authors wish to express their gratitude to Dr N. G. Needham for his help with metallographic investigations.

References

Ainsworth, R. A. 1982 Some observations on creep crack growth. *Int. J. Fracture* **18**, 26.

American Society for Mechanical Engineers 1977 code case N47. Interpretations of A.S.M.E. boiler and pressure vessel code.

Ashby, M. F. 1972 A first report on deformation-mechanism maps. *Acta metall.* **20**, 887.

PHILOSOPHICAL TRANSACTIONS OF THE ROYAL SOCIETY A MATHEMATICAL, PHYSICAL & ENGINEERING SCIENCES

Boettner, R. C. & Robertson, W. D. 1961 Study of the growth of voids in copper during the creep process by measurement of accompanying change in density. *Trans. metall. Soc. A.I.M.E.* **221**, 613.

Bridgman, P. W. 1952 *Studies in large plastic flow and fracture*. New York: McGraw-Hill.

British Standard 1969 no. 3500, part I. Methods for creep rupture testing of materials.

British Standard 1982 no. 5500. Specification for unfired fusion welded pressure vessels.

Brown, D. R., Hancock, J. W., Thomson, R. & Parks, D. M. 1980 The effect of dilating plasticity on some elastic-plastic stress and strain concentration problems relevant to fracture. *Numerical methods in fracture mechanics* (*Proc. 2nd Int. Conf. Univ. Coll., Swansea, Wales*) (ed. D. R. J. Owen & A. R. Luxmoore), p. 304. Swansea: Pineridge.

Chaboche, J.-L. 1979 Le concept de contrainte effective appliqué a l'elasticité et la viscoplasticite en presence d'un endommagement anisotrope. (Presented to the Euromech Congress 115, Grenoble, 19–22 June.) Also ONERA Rep. no. 1979–77, Chatillon, Paris.

Cocks, A. C. F. & Ashby, M. F. 1982*a* On creep fracture by void growth. *Prog. Mater. Sci.* **27**, 189.

Cocks, A. C. F. & Ashby, M. F. 1982*b* The growth of a dominant crack in a creeping material. *Scr. metall.* **16**, 109.

Dyson, B. F. 1976 Constraints on diffusional cavity growth rates. *Metal. Sci.* **10**, 349.

Dyson, B. F. 1978 Constrained cavity growth, its use in quantifying recent fracture results. *Can. metall. Q.* **18**, 31.

Dyson, B. F. & Loveday, M. S. 1981 Creep fracture in Nimonic 80A under tri-axial tensile stressing. *Creep in structures*, 1980 (*I.U.T.A.M. Symposium, Leicester, U.K.*) (ed. A. R. S. Ponter & D. R. Hayhurst), p. 406. Berlin: Springer-Verlag.

Ewing, D. J. F. & Hill, R. 1967 The plastic constraint of *V*-noted tension bars. *J. Mech. Phys. Solids* **15**, 115.

Hayhurst, D. R. 1972 Creep rupture under multi-axial states of stress. *J. Mech. Phys. Solids* **20**, 381.

Hayhurst, D. R. 1973 Stress redistribution and rupture due to creep in a uniformly stretched thin plate containing a circular hole. *J. appl. Mech.* **40**, 244.

Hayhurst, D. R. 1976 Estimates of the creep rupture lives of structures subjected to cyclic loading. *Int. J. mech. Sci.* **18**, 75.

Hayhurst, D. R. & Brown, P. R. 1984 The use of finite element creep solutions to obtain *J* integrals for plane strain cracked member. *Int. J. mech. Sci.* **26**, 29.

Hayhurst, D. R., Dimmer, P. R. & Chernuka, M. W. 1975*a* Estimates of the creep rupture lifetime of structures using the finite element method. *J. Mech. Phys. Solids* **23**, 335.

Hayhurst, D. R., Dimmer, P. R. & Morrison, C. J. 1984 Development of continuum damage in the creep rupture of notched bars. *Phil. Trans. R. Soc. Lond.* A **311**, 103–129.

Hayhurst, D. R., Leckie, F. A. & Morrison, C. J. 1978 Creep rupture of notched bars. *Proc. R. Soc. Lond.* A **360**, 243.

Hayhurst, D. R., Morrison, C. J. & Brown, P. R. 1981 Creep crack growth. *Creep in structures*, 1980 (*I.U.T.A.M. Symposium, Leicester, U.K.*) (ed. A. R. S. Ponter & D. R. Hayhurst), p. 564. Berlin: Springer-Verlag.

Hayhurst, D. R., Morrison, C. J. & Leckie, F. A. 1975*b* The effect of stress concentrations on the creep rupture of tension panels. *J. appl. Mech.* **42**, 613.

Hayhurst, D. R., Trampczynski, W. A. & Leckie, F. A. 1980 Creep rupture under non-proportional loading. *Acta metall.* **28**, 1171.

Hayhurst, D. R., Trampczynski, W. A. & Leckie, F. A. 1983 On the rôle of cavity nucleation in creep deformation and fracture. *Acta metall.* **31**, 1537.

Harper, M. P. & Ellison, E. G. 1977 The use of the C^* parameter in predicting creep crack propagation rates. *J. Strain Anal.* **12** (3), 167.

Hui, C. Y. & Riedel, H. 1981 The asymptotic stress and strain fields near the tip of a growing crack under creep conditions. *Int. J. Fracture* **17** (4), 409.

Hutchinson, J. W. 1968 Singular behaviour at the end of a tensile crack in a hardening material. *J. Mech. Phys. Solids* **16**, 13.

Hutchinson, J. W. 1983 Constitutive behaviour and crack tip fields for materials undergoing creep-constrained grain boundary cavitation. *Acta metall.* **31**, no. 7, 1079.

Kachanov, L. M. 1960 *The theory of creep* (English translation ed. A. J. Kennedy), chs IX, X. Boston Spa, Wetherby: British Library.

Landes, J. D. & Begley, J. 1976 A fracture mechanics approach to creep crack growth. Mechanics of crack growth, A.S.T.M. STP no. 59. American Society for Testing and Materials.

Leckie, F. A. & Hayhurst, D. R. 1975 The damage concept in creep mechanics. *Mech. Res. Commun.* **2**, 23.

Leckie, F. A. & Hayhurst, D. R. 1977 Constitutive equations for creep rupture. *Acta metall.* **25**, 1059.

Leckie, F. A. & Hayhurst, D. R. 1981 Experiments in high temperature fracture, Dep. Rep. no. 104, Design and Materials Division, dept Mech. & Ind. Eng., University of Illinois, Urbana, Champaign, U.S.A.

McMeeking, R. M. 1977 Finite deformation analysis of crack-tip opening in elastic-plastic materials and implications for fracture. *J. Mech. Phys. Solids* **25**, 357.

Nagtegaal, J. C., Parks, D. M. & Rice, J. R. 1974 On numerically accurate finite element solutions in the fully plastic range. *Comput. Meth. appl. Mech. Engng* **4**, 153.

Neate, G. J. 1977 Creep crack growth in 1½% Cr–½% Mo–¼% V steel at 565 °C. *Engng Fracture Mech.* **9**, 297.

PHILOSOPHICAL TRANSACTIONS OF THE ROYAL SOCIETY A MATHEMATICAL, PHYSICAL & ENGINEERING SCIENCES

Neate, G. J. & Siverns, M. J. 1973 The application of fracture mechanics to creep crack growth. *Proc. Int. Conf. on Creep and Fatigue in Elev. Temp. Applics, Philadelphia and Sheffield.* Joint A.S.M.E.–I.Mech.E., paper C234/73, vol. 1. London: I. Mech. E.

Needham, N. G. & Gladman, T. 1980 The effect of stress-state on the processes controlling creep fracture in a $2\frac{1}{4}\%$ Cr 1% Mo steel. *Proc. Int. Conf. on Engng aspects of Creep*, 15–19 *Sept.* 1980, *Sheffield*, **1**, paper C190/80, p. 49. London: Institute of Mechanical Engineers.

Ohtani, R. 1981 *Finite element analysis and experimental investigation on creep crack propagation* (*I.U.T.A.M. Symposium, Leicester, U.K.*) (ed. A. R. S. Ponter & D. R. Hayhurst), p. 542. Berlin: Springer-Verlag.

Rabotnov, Yu. M. 1969 *Creep problems in structural members* (English translation ed. F. A. Leckie), ch. 6. Amsterdam: North Holland.

Raj, R. & Ashby, M. F. 1975 Intergranular fracture at elevated temperature. *Acta metall.* **23**, 653.

Rice, J. R. 1968 A path independent integral and the approximate analysis of strain concentration by notches and cracks. *J. appl. Mech.* **35**, 379.

Rice, J. R. & Rosengren, G. F. 1968 Plane strain deformation near a crack tip in a power law hardening material. *J. Mech. Phys. Solids* **16**, 1.

Riedel, H. 1978 Cracks under creep conditions. *Z. Metallk.* **69** (12), 755.

Riedel, H. 1981 *The extension of a macroscopic crack at elevated temperature by the growth and coalescence of microvoids* (*I.U.T.A.M. Symposium, Leicester, U.K.*) (ed. A. R. S. Ponter & D. R. Hayhurst), p. 504. Berlin: Springer-Verlag.

Riedel, H. & Rice, J. R. 1980 Tensile cracks in creeping solids. *ASTM 12th Annual National Symposium on Fracture Mechanics, St Louis, May* 1979. A.S.T.M. STP 700, 112.

Tada, H., Paris, D. & Irwin, G. 1973 *The stress analysis of cracks handbook.* Hellertown, U.S.A.: Del. Res. Corp.

Taira, S., Ohtani, R. & Kitamura, T. 1979 Application of *J*-integral to high-temperature crack propagation, Part I – creep crack propagation. *J. engng Mat. Tech.* **101**, 154.

Vavakin, A. S. & Salganik, R. L. 1975 Effective characteristics of non homogeneous media with isolated inhomogeneities. *Izv. Akad. Nauk SSSR*, Mekhanika Tverdogo Tela, **10** (3), 65.

Webster, G. A. 1975 The application of fracture mechanics to creep cracking. *Proc. Conf. Mech. and Physics of Fracture, January* (*Cambridge, U.K.*), paper 18. London: Institute of Physics.

PHILOSOPHICAL TRANSACTIONS OF THE ROYAL SOCIETY A MATHEMATICAL, PHYSICAL & ENGINEERING SCIENCES

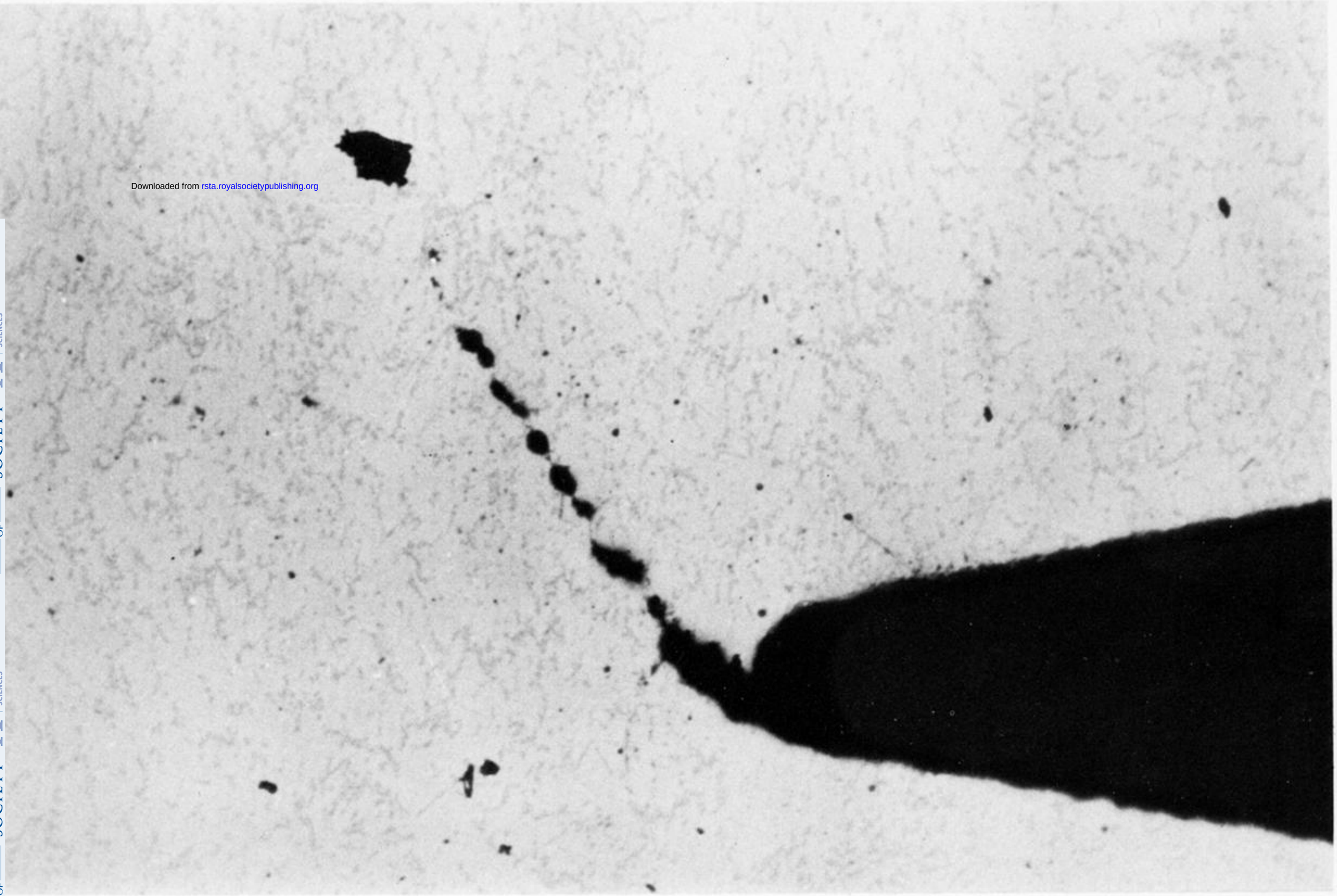

FIGURE 3. Crack tip shear damage, close to failure, in an externally cracked specimen made from D19S aluminium alloy and tested at 150 °C (magnification ×90).

PHILOSOPHICAL TRANSACTIONS OF THE ROYAL SOCIETY A MATHEMATICAL, PHYSICAL & ENGINEERING SCIENCES

(a)

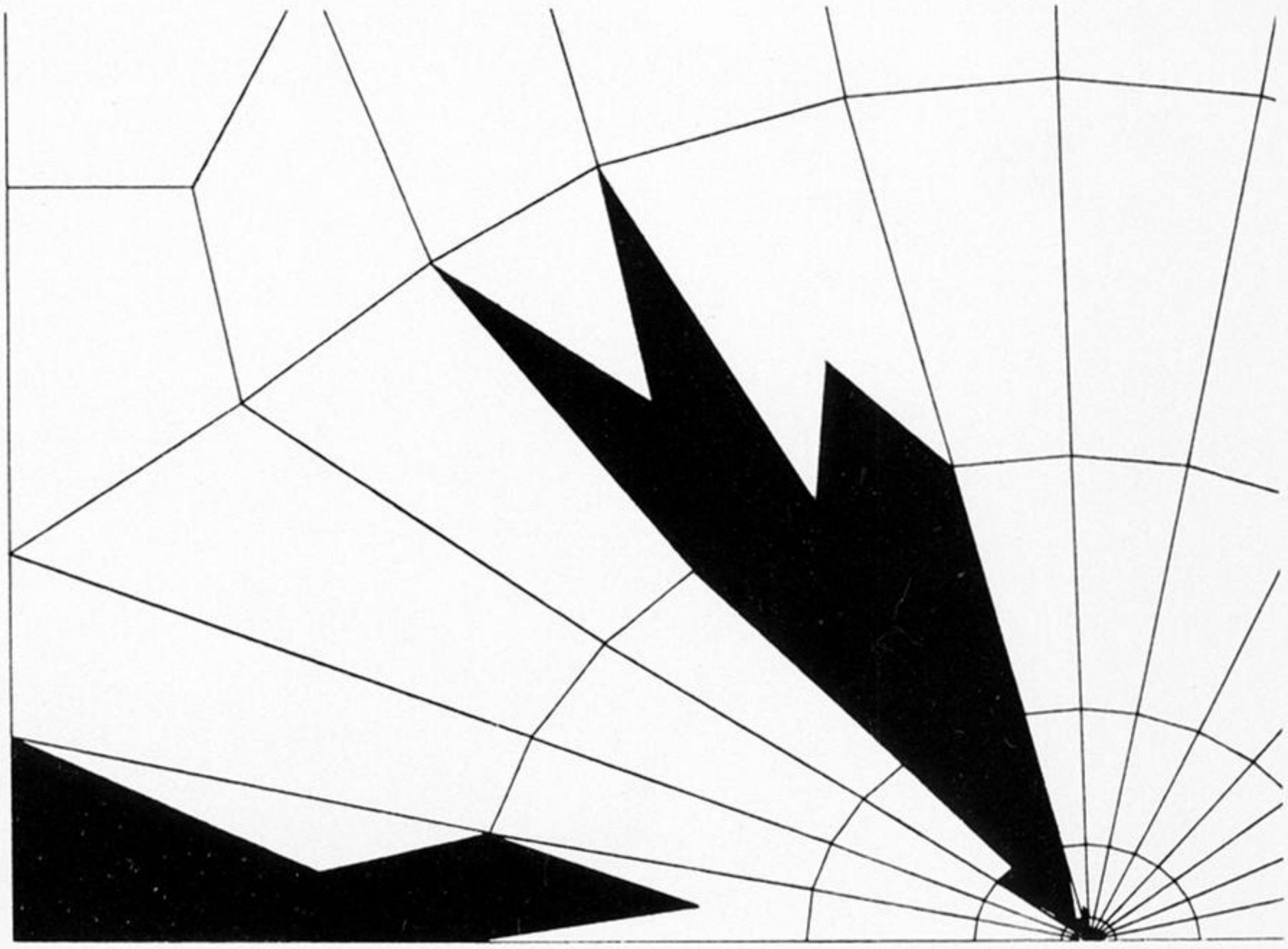

(b)

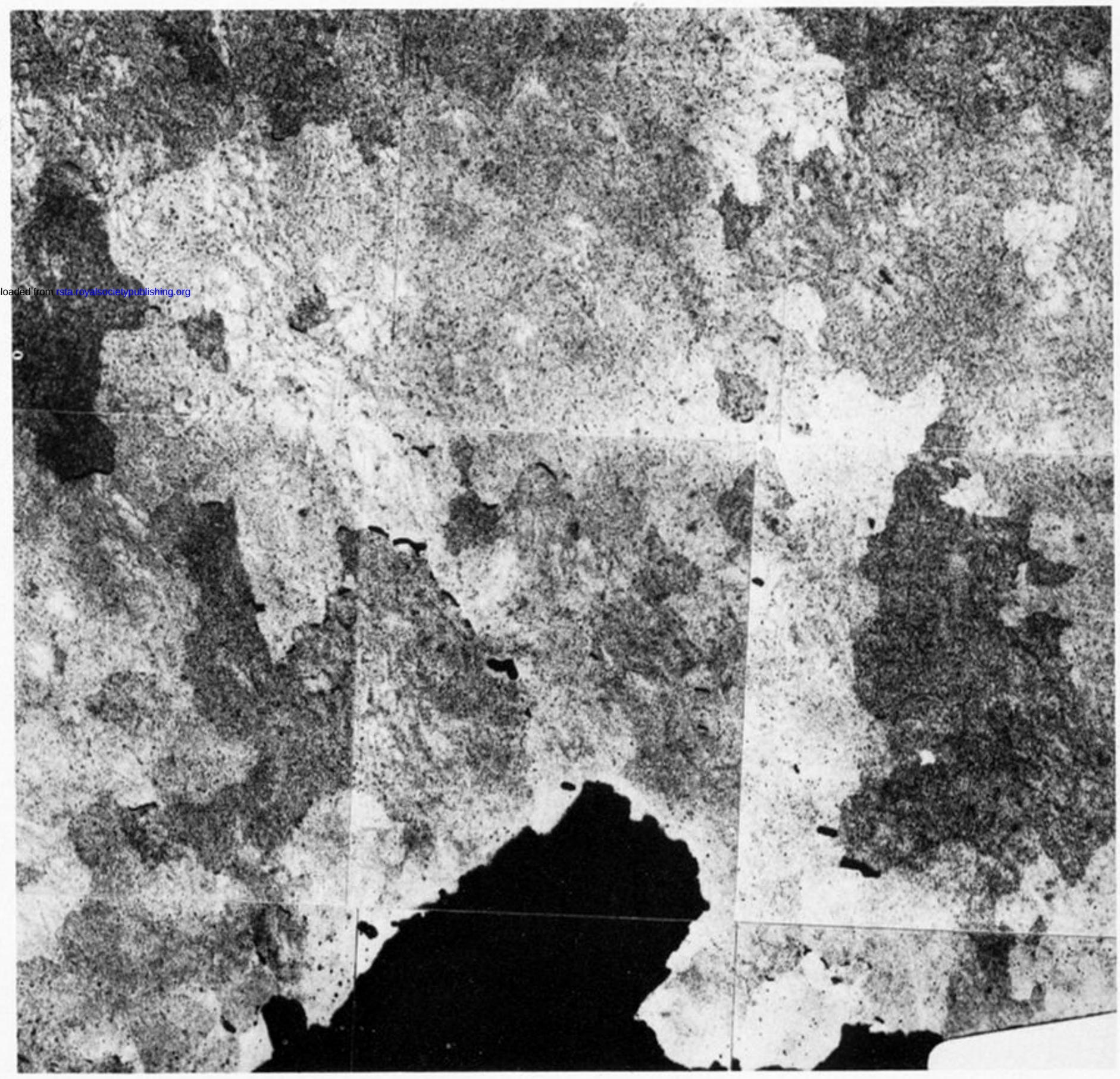

FIGURE 6. Comparison of (*a*) computed failure path, $\omega \geqslant 0.999$, with (*b*) mid-thickness micrograph taken from the minimum section of an externally cracked specimen in an aluminium alloy at failure. Original crack profile shown in white.

(a)

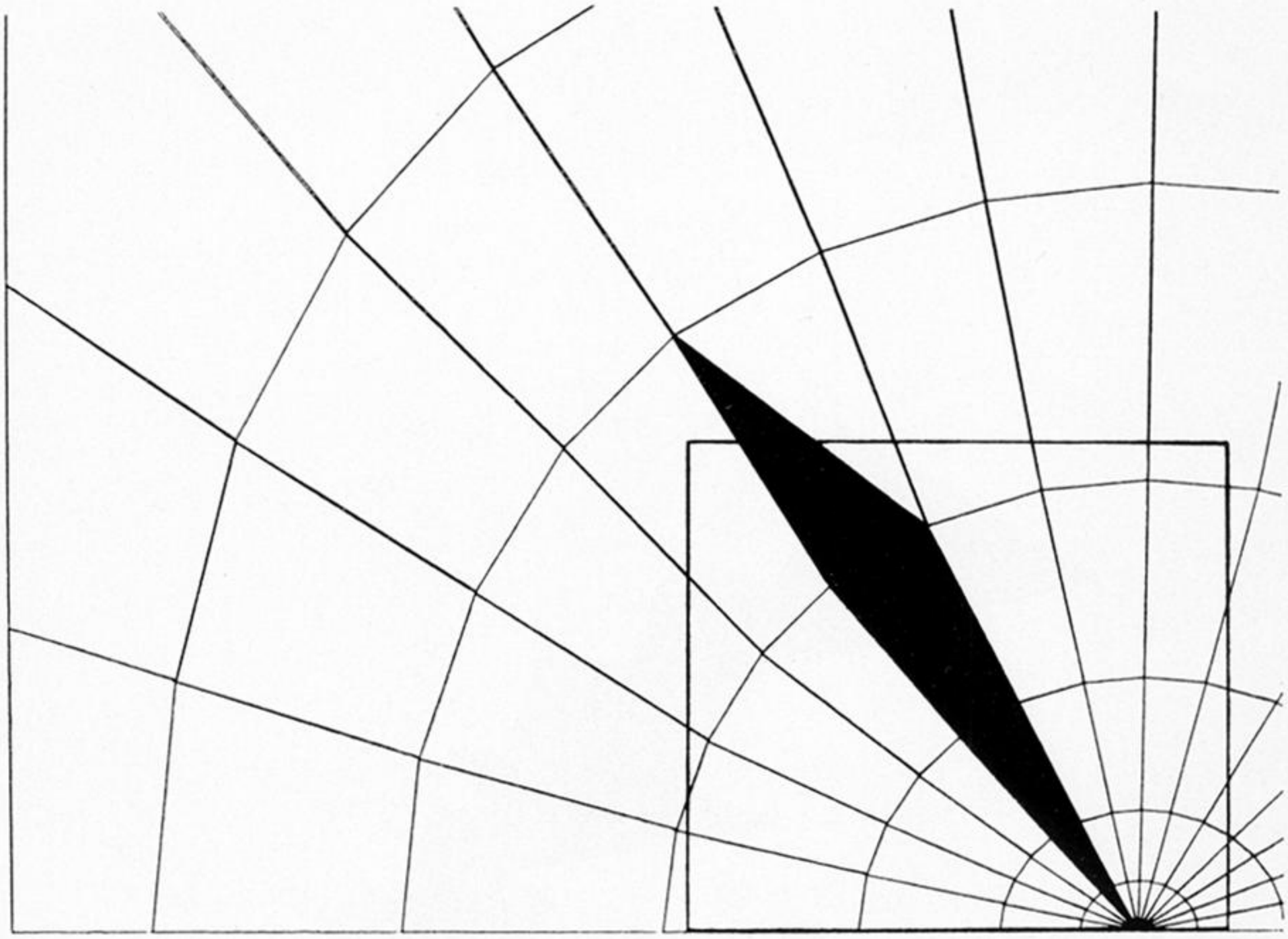

(b)

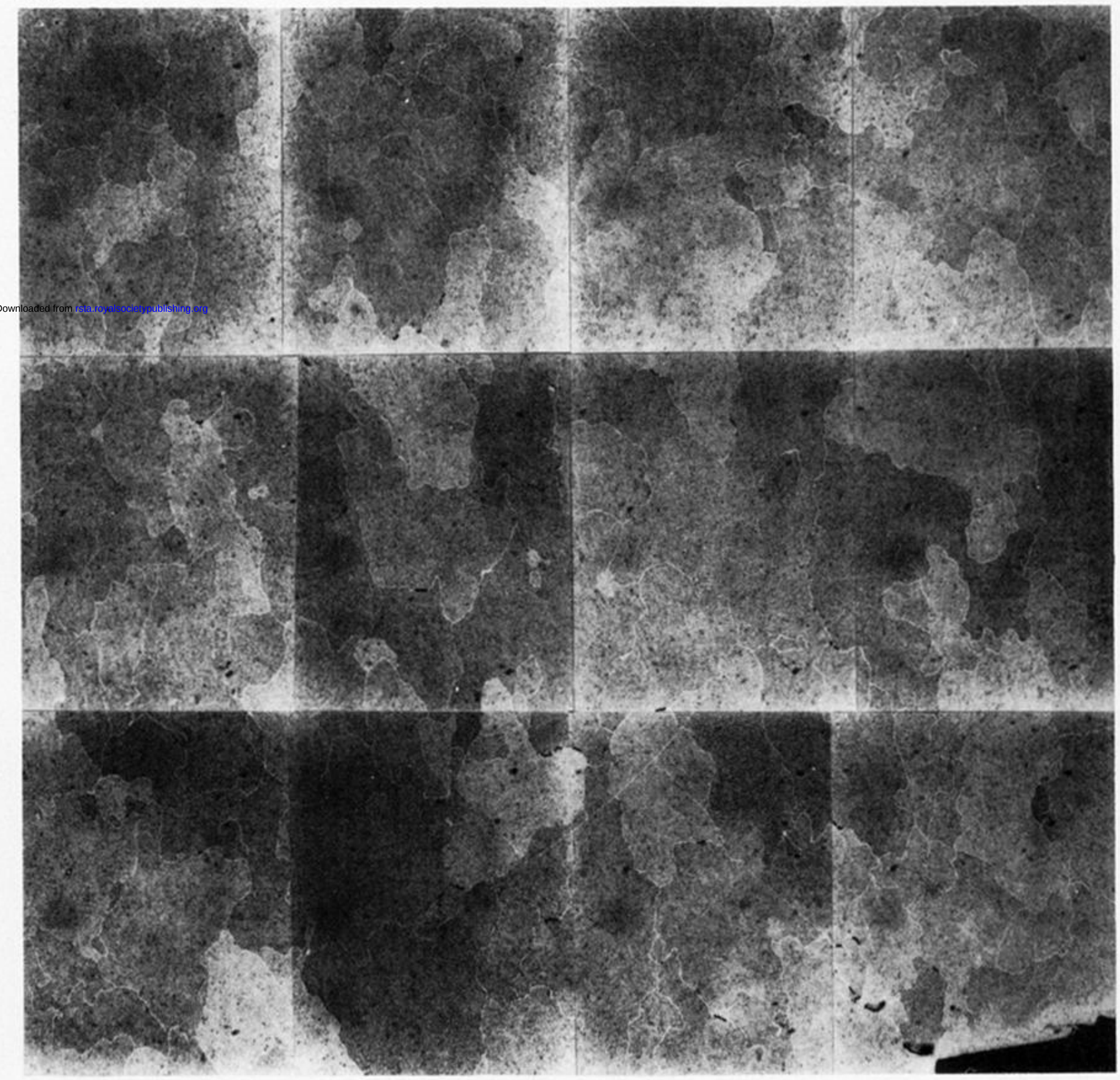

FIGURE 7. Comparison of (*a*) computed failure path, $\omega \geqslant 0.999$, for the minimum section with (*b*) a mid-thickness micrograph taken from a selected region of an internally cracked specimen in an aluminium alloy at $t/t_t = 0.95$.

(a)

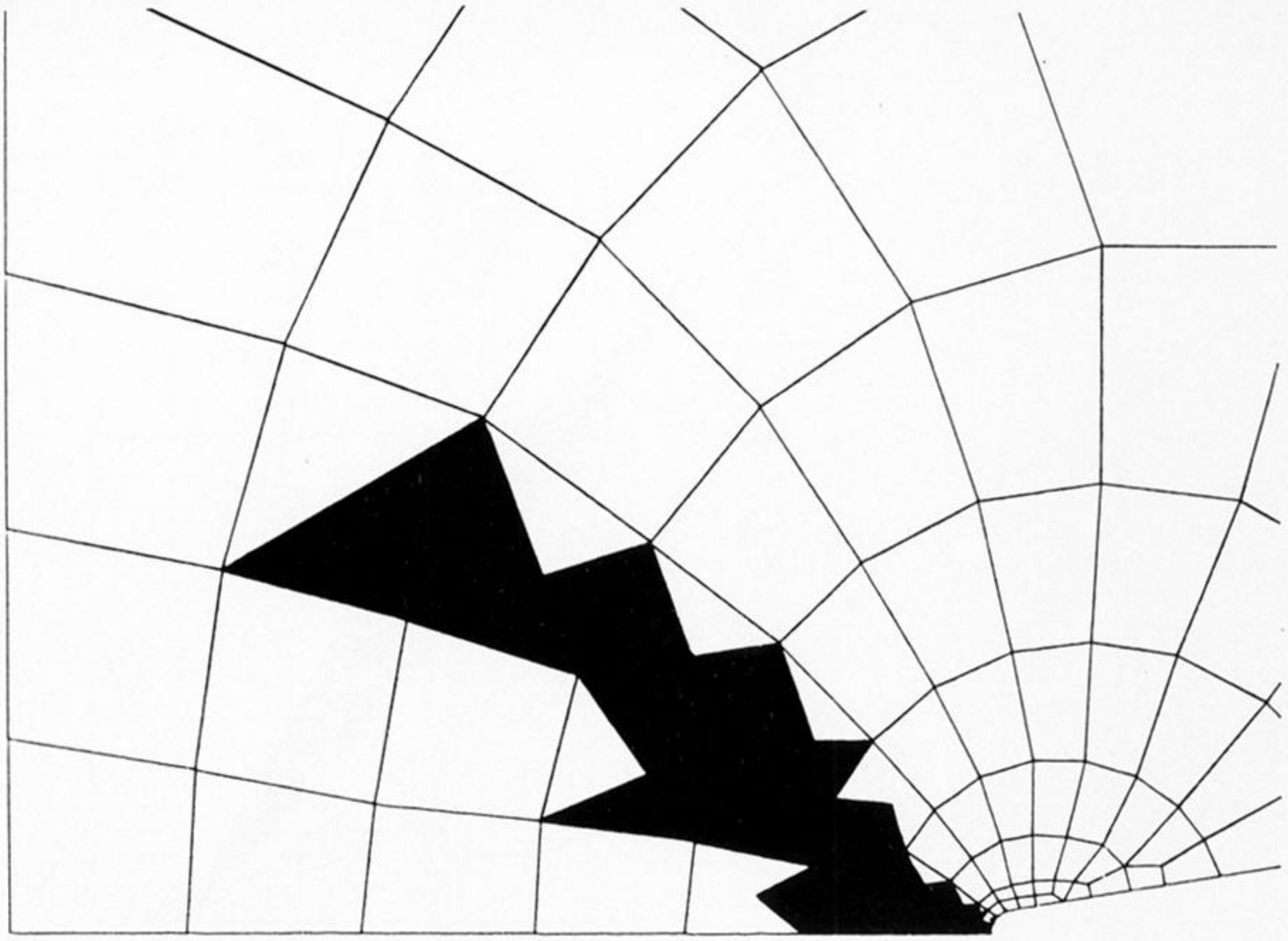

(b)

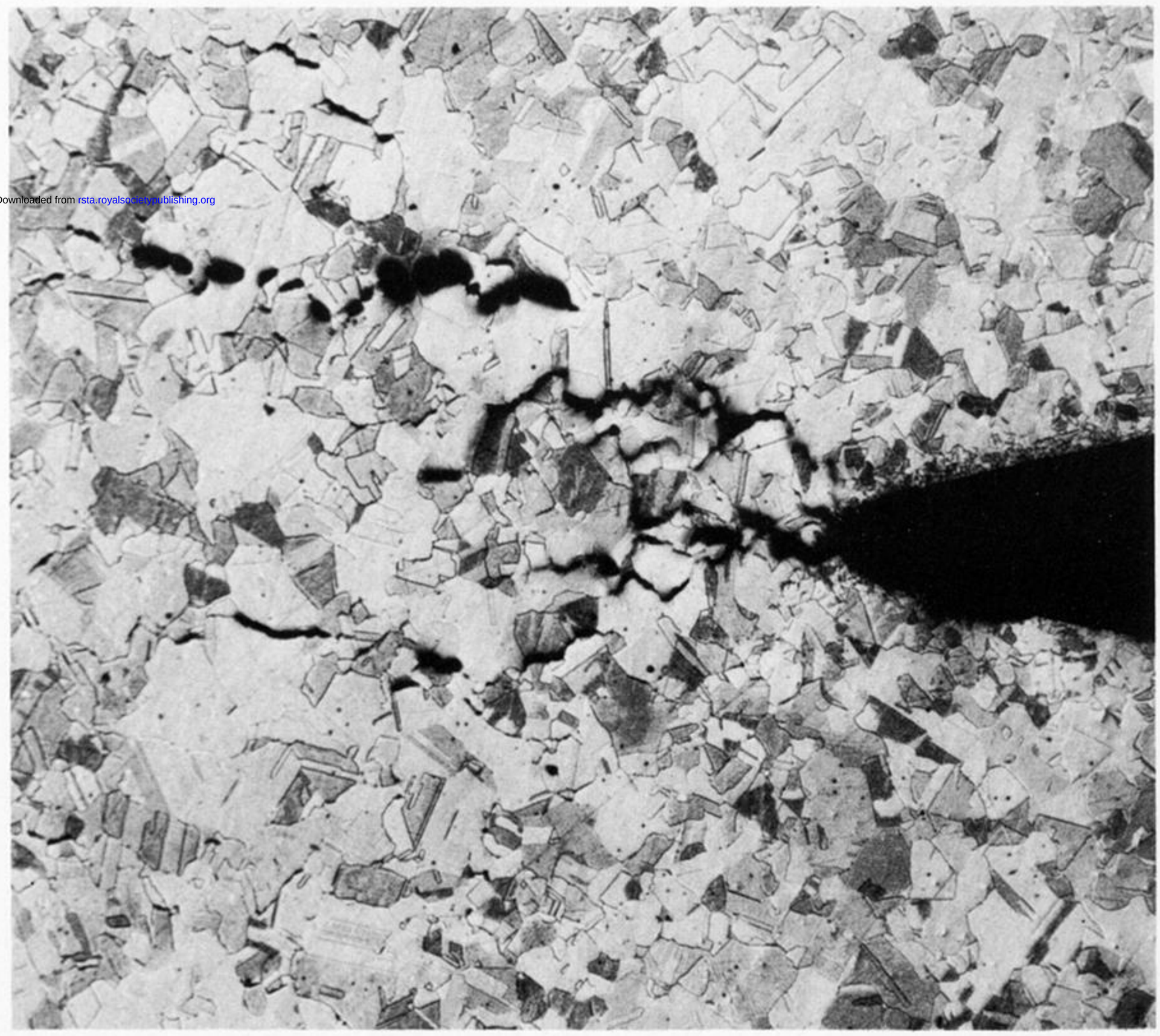

FIGURE 11. Comparison of (*a*) computed failure path, $\omega \geqslant 0.999$, with (*b*) mid-thickness micrograph taken from the minimum section of an externally cracked specimen in copper at $t/t_t = 0.94$.

(a)

(b)

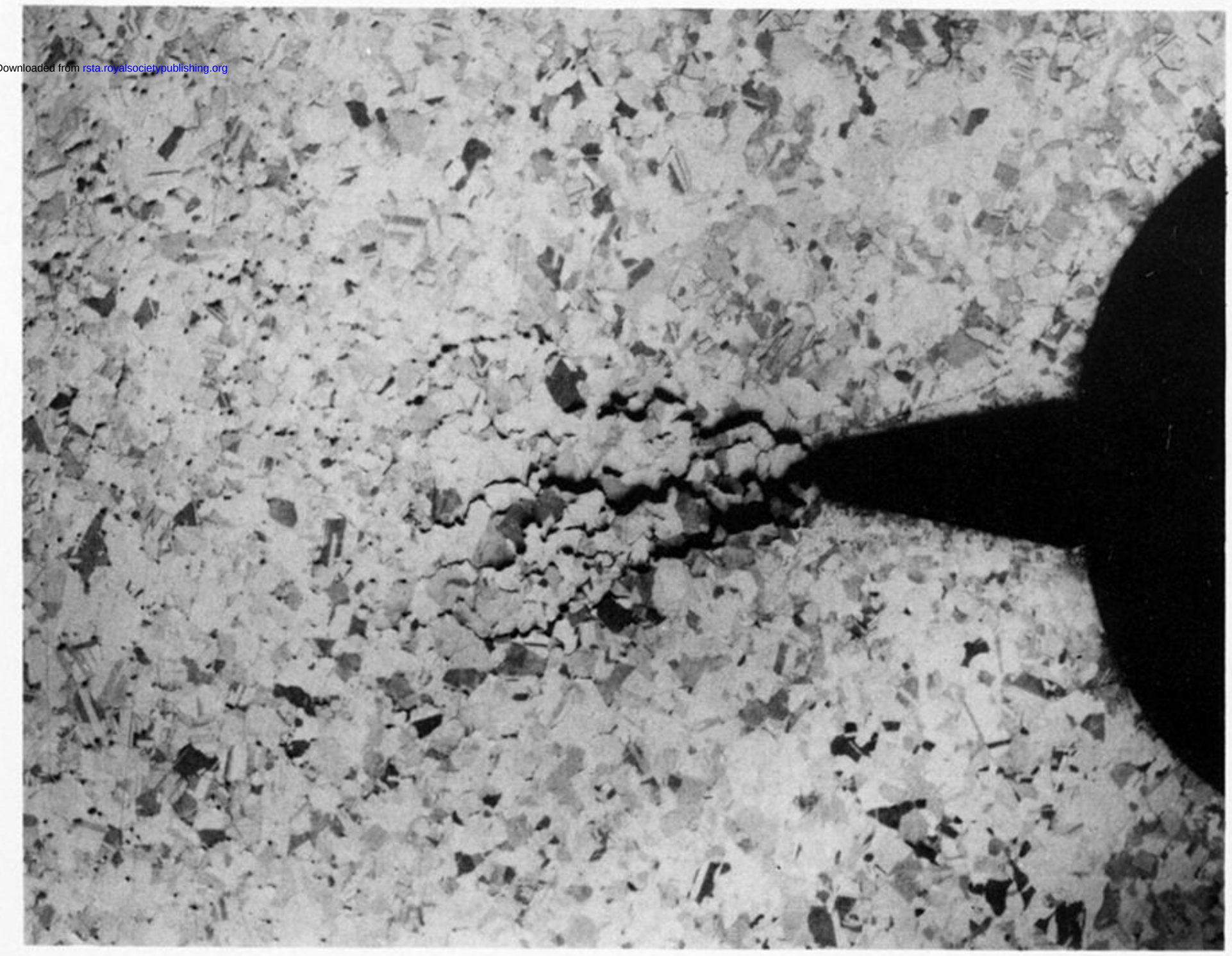

FIGURE 12. Comparison of (*a*) computed failure path, $\omega \geqslant 0.999$, with (*b*) mid-thickness micrograph taken from the minimum section of an internally cracked specimen in copper at $t/t_f = 0.99$.

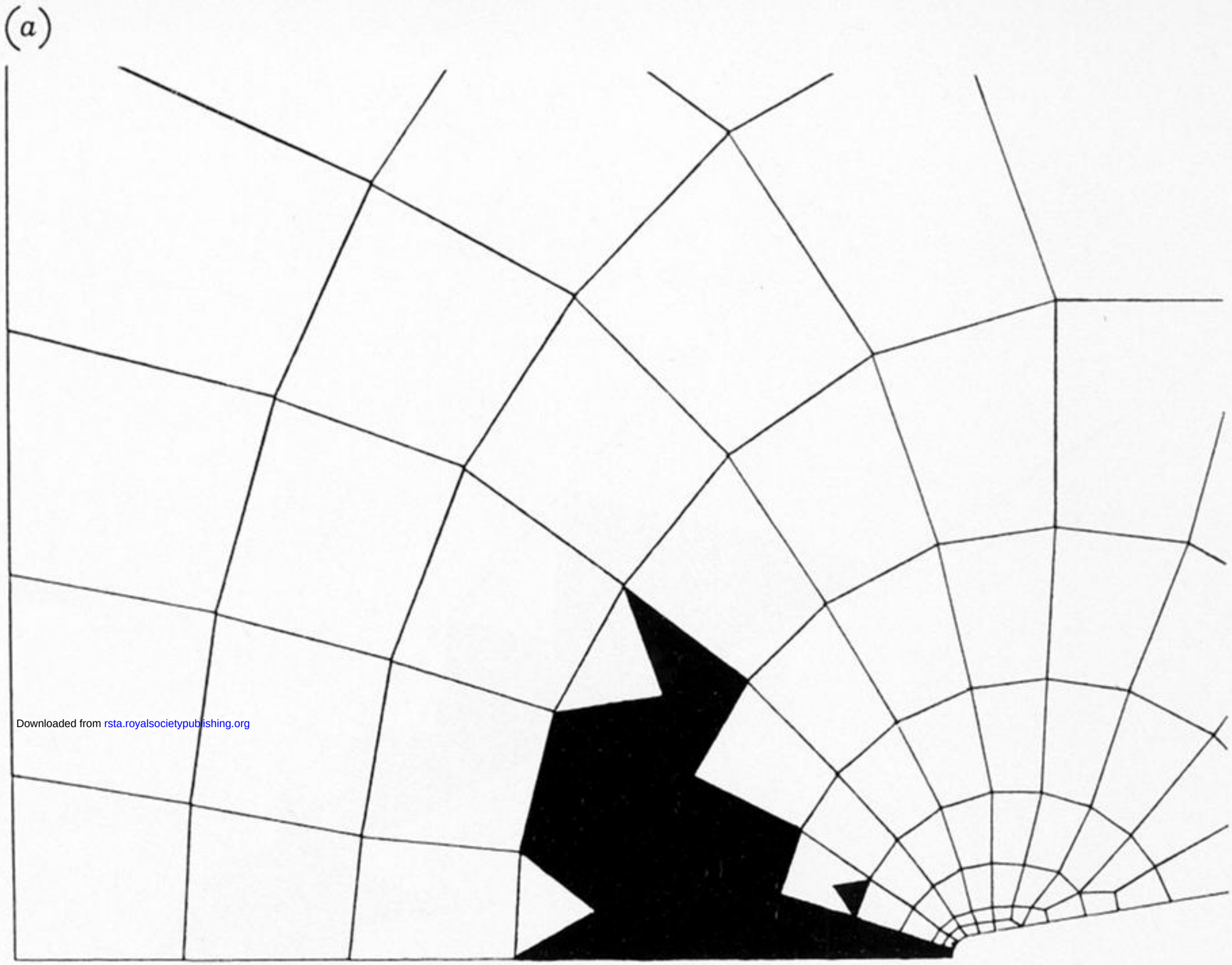

IGURE 16. Comparison of (*a*) computed failure path, $\omega \geqslant 0.999$, with (*b*) mid-thickness micrograph taken from the minimum section of an externally cracked specimen in 316 stainless steel at $t/t_t = 0.6$.

(a)

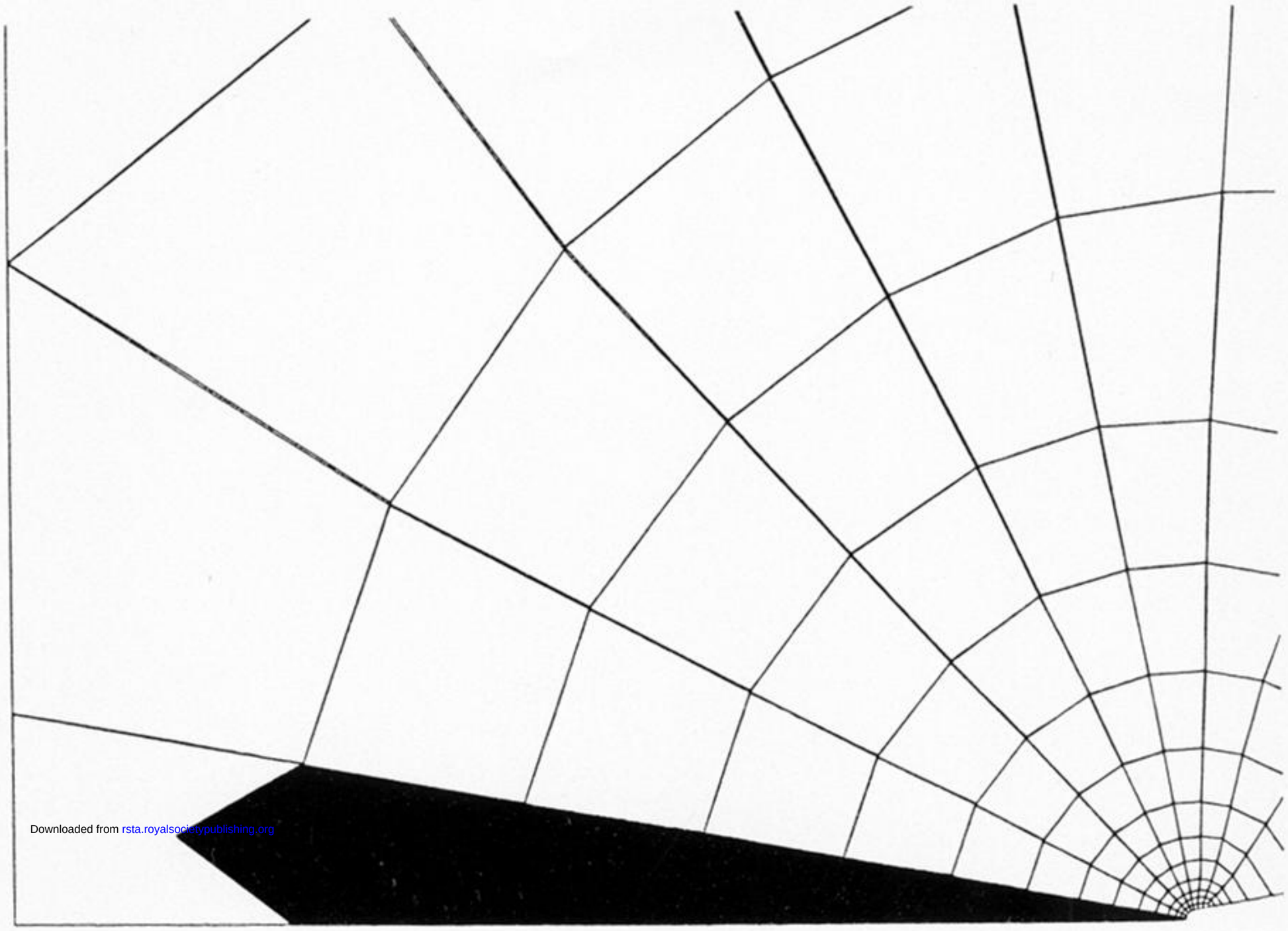

(b)

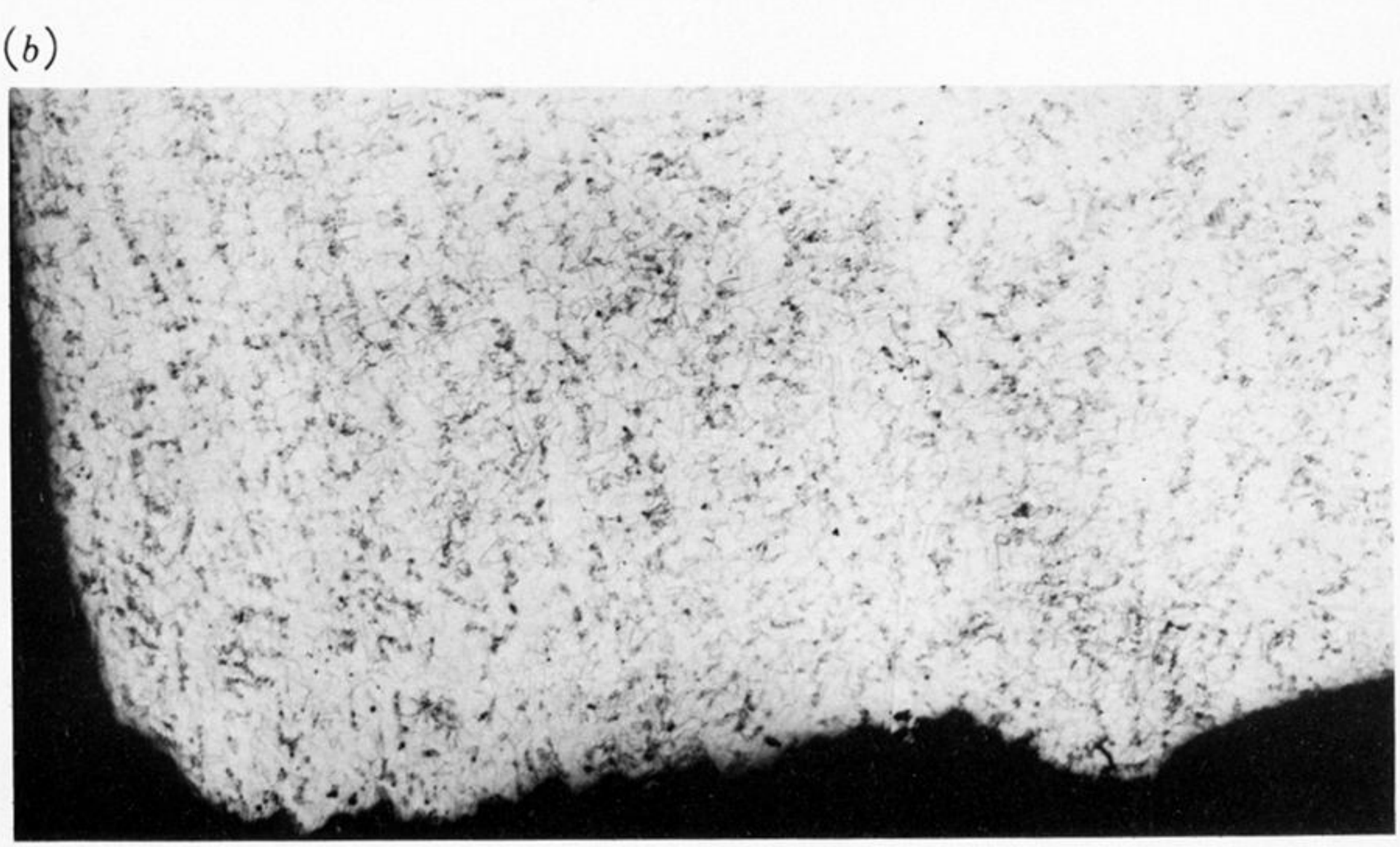

FIGURE 17. Comparison of (*a*) computed failure path, $\omega \geqslant 0.999$, with (*b*) mid-thickness micrograph taken from the minimum section of an internally cracked specimen in 316 stainless steel at failure.